Moment functional based spectral density functional theory

Frank Freimuth [1,2,*] Stefan Blügel [1] and Yuriy Mokrousov [1,2]

[1] *Peter Grünberg Institut and Institute for Advanced Simulation, Forschungszentrum Jülich and JARA, 52425 Jülich, Germany*

[2] *Institute of Physics, Johannes Gutenberg University Mainz, 55099 Mainz, Germany*

(Received 28 July 2022; revised 23 September 2022; accepted 26 September 2022; published 6 October 2022)

We describe a density functional method which aims at computing the ground state electron density and the spectral function at the same time. One basic ingredient of our method is the construction of the spectral function from the first four spectral moment matrices. The second basic ingredient is the construction of the spectral moment matrices from density functionals. We call our method moment functional based spectral density functional theory (MFbSDFT), because it is based on density functionals for the spectral moments and because it allows us to compute the spectral function. If it is implemented in second variation our method consumes only a fraction more computer time than a standard DFT calculation with the PBE functional. We show that MFbSDFT captures correlation effects such as the valence-band satellite in Ni and the formation of lower and upper Hubbard bands in $SrVO_3$. For the purpose of constructing the spectral function from the first four $N \times N$ spectral moment matrices we describe an efficient algorithm based on the diagonalization of one Hermitian $2N \times 2N$ matrix.

DOI: 10.1103/PhysRevB.106.155114

I. INTRODUCTION

In density functional theory (DFT) the ground state electron density is determined by minimizing the total energy functional [1]. While most contributions to the total energy functional, such as the Hartree energy, the exchange energy, and the correlation energy, can be expressed as functionals of the electron density, it is difficult to express the kinetic energy directly in this way. This is why within the most popular kind of DFT—the Kohn-Sham (KS) DFT—the KS-Hamiltonian [2] is set up and solved with the main purpose to provide the kinetic energy.

However, the KS energy bands agree very often fairly well with photoemission data [3] and the KS spectrum is therefore even used to compute response properties such as the anomalous Hall effect [4], the Gilbert damping [5], the direct and inverse spin-orbit torque [6], and the inverse Faraday effect [7] in metallic systems. These KS response functions are often in good agreement with the corresponding material property tensors measured experimentally.

Well-known deficiencies of this approach are the underestimation of the band gap, which may require the application of band shifts when computing optical responses such as photocurrents [8] in semiconductors such as GaAs. Instead of shifting the bands to match the band gap known from experiments, one may use the *GW* approximation [9], which is a parameter-free technique based on many-body perturbation theory and which often predicts gaps that are closer to experiment than KS-DFT. However, since one deals then directly with a many-body Hamiltonian, one forsakes the DFT idea of obtaining all properties as directly as possible from the ground state density in order to avoid the complexity and factorial growth of the many-body Hilbert space. Another short coming of KS spectra is the overestimation of the magnetic moment and the resulting overestimation of the exchange splitting of some weak itinerant ferromagnets such as MnSi, which requires us to reduce the exchange field by a scaling factor in order to compute the topological Hall effect in MnSi [10].

Moreover, a well-known deficiency of the KS spectrum is the absence of the splitting of bands into lower and upper Hubbard bands due to strong electron correlations [11]. Such a splitting of the single-particle bands leads, for example, to the appearance of a satellite peak roughly 6 eV below the Fermi energy in Ni [12–14]. In order to compute the spectrum in such cases of strongly interacting electrons one often uses DFT only to obtain the KS wave functions of a small manifold corresponding to a small energy window around the Fermi energy and constructs an interacting Hamiltonian for this manifold, which one solves by dynamical mean-field theory (DMFT) [15,16] in order to obtain the spectral function. In other words, one remains within the DFT-framework in order to determine the ground state density, but similarly to *GW* one leaves this framework and directly solves an interacting many-electron Hamiltonian in order to obtain the spectrum of the correlated system instead of evaluating a density functional. However, one may also take a different viewpoint: The local spectral function of DMFT minimizes the effective action. In this sense, DMFT is a spectral density functional approach [16].

Nevertheless, the question still poses itself if it is possible to obtain both ground state density and correlated spectral function within a density functional approach which avoids the direct use of many-body techniques such as *GW* and DMFT. A Hermitian $N \times N$ matrix has N real-valued eigenvalues. This well-known fact from linear algebra is exploited in many electronic structure programs based on density functional theory, where the KS equations are solved numerically

*f.freimuth@fz-juelich.de

by diagonalizing a Hermitian matrix. The direct construction of $2N$ state vectors, $2N$ state energies, and $2N$ spectral weight factors from four Hermitian $N \times N$ spectral moment matrices [17] may be considered as a generalization of the diagonalization of Hermitian matrices. It may also be interpreted as a generalization of the two-pole approximation [18,19] used in the self-consistent spectral moment method of the single-band Hubbard model to the case of many bands [17]. Since the self-consistent moment method based on the first four spectral moments captures the Ni satellite peak [13], such a generalization may be useful when the description of the spectral properties obtained from standard DFT needs to be improved because of strong correlation effects, which split the electronic bands into lower and upper Hubbard bands.

The Ith spectral moment matrix is defined by [13,17,18,20]

$$\boldsymbol{M}_{\sigma}^{(I)} = \frac{1}{\hbar}\int_{-\infty}^{\infty} \boldsymbol{S}_{\sigma}(E) E^{I} dE, \tag{1}$$

where $\boldsymbol{S}_{\sigma}(E)$ is the spectral density matrix at energy E. In this paper, we discuss only the magnetically collinear case without spin-orbit coupling. Therefore there are only spectral density matrices $\boldsymbol{S}_{\uparrow}(E)$ with spin $\sigma = \uparrow$ and spectral density matrices $\boldsymbol{S}_{\downarrow}(E)$ with spin $\sigma = \downarrow$. So far, the direct construction of the spectral function of interacting fermionic many-particle systems from the first four spectral moments has not yet been investigated intensively. Well-explored are only the single-band case with the first four spectral moments [18,19], the many-band case with the first two spectral moments [21], which has been shown to provide a Hartree-Fock type approximation, and the option to use the spectral moments as sum rules in order to guide the construction of the spectral function by other means [22]—a concept which one may extend even to nonequilibrium conditions [23].

Recently, we have demonstrated how to solve the Hubbard-Rashba model within the many-band generalization of the two-pole approximation of the spectral density and of the self-consistent moment method [17]. For this purpose, we did not make use of the DFT concept, but instead we computed the higher-order correlation functions $\langle c_{i\alpha}^{\dagger} c_{j\beta}^{\dagger} c_{l\gamma} c_{m\delta} \rangle$ self-consistently based on the spectral theorem [24]. Such higher-order correlation functions are needed to compute the spectral moment $\boldsymbol{M}_{\sigma}^{(3)}$, for example. While the spectral moment matrices $\boldsymbol{M}_{\sigma}^{(I)}$ all have two orbital indices, the higher-order correlation functions such as $\langle c_{i\alpha}^{\dagger} c_{j\beta}^{\dagger} c_{l\gamma} c_{m\delta} \rangle$ have at least four orbital indices. The computational effort of standard KS DFT scales with the third power of the number of basis functions N_{B}. Obviously, the many-band self-consistent moment method scales worse, namely at least $\propto N_{\mathrm{B}}^{4}$. In order to keep the computational effort low, we therefore proposed in Ref. [17] to map the KS electronic structure of the valence bands and the first few conduction bands first onto Wannier functions. The resulting Wannier Hamiltonian may then be supplemented by Hubbard-type interactions and this interacting Hamiltonian may be treated with the many-band generalization of the self-consistent moment method. However, similarly to the *GW* and LDA+DMFT approaches discussed above, one thereby leaves the DFT framework, because one computes the spectrum using a many-body Hamiltonian technique instead of a density functional.

In this paper, we combine basic ideas of DFT with the many-band generalization of the self-consistent moment method in order to develop an approach which aims at computing both the ground state density and the spectral function at the same time without forsaking the DFT framework. The first Hohenberg-Kohn theorem states that the ground state electron density determines the Hamiltonian up to a constant. Since the spectral moments can be computed from the Hamiltonian, the Hohenberg-Kohn theorem implies therefore that also the spectral moments may be expressed as density functionals. To explore how this can be done in practice is the central goal of this paper. Combining this with our recipe [17] to construct the spectral function from the first four spectral moments we obtain a moment functional based spectral density functional theory (MFbSDFT).

The rest of this paper is structured as follows. In Sec. II, we explain the theory of MFbSDFT. In Sec. III, we describe an efficient algorithm for computing the spectral function from the first four spectral moments. In Sec. IV, we explain how we construct the moment functionals. In Sec. V, we explain how the MFbSDFT method may be implemented within the full-potential linearized augmented plane wave method (FLAPW) within a second variation approach. In Sec. VI, we present applications of our method to fcc Ni and $SrVO_3$. In Sec. VII, we discuss some open questions of MFbSDFT and strategies of how to develop it further. This paper ends with a summary in Sec. VIII.

II. THEORY

A. The concept of moment functionals

The ground state charge density defines the Hamiltonian uniquely (up to a constant) [1]. Consequently, it determines also the spectral function uniquely. In order to write the spectral function in matrix form we need a suitable set of orthonormal basis functions $\phi_n(\boldsymbol{r})$. Denoting the creation and annihilation operators corresponding to state $\phi_n(\boldsymbol{r})|\sigma\rangle$—where $|\sigma\rangle$ is a spinor—by $c_{\sigma n}^{\dagger}$ and $c_{\sigma n}$, respectively, the matrix elements of the spectral function matrix are

$$S_{\sigma nm}(E) = \frac{1}{2\pi}\int dt\, e^{\frac{i}{\hbar}Et} \langle [c_{\sigma n}(t), c_{\sigma m}^{\dagger}]_{+} \rangle. \tag{2}$$

When periodic boundary conditions are used, the spectral function and the spectral moments aquire an additional $\boldsymbol{k}$-index for the k point $\boldsymbol{k}$, which we often suppress in this manuscript for notational convenience.

The spectral moments may be obtained by plugging Eq. (2) into Eq. (1). Since the spectral function is uniquely determined by the ground state density, also the spectral moments are uniquely defined by it. The spectral moments may also be expressed in terms of real-space coordinates:

$$M_{\sigma}^{(I)}(\boldsymbol{r}, \boldsymbol{r}') = \frac{1}{\hbar}\int dE E^{I} \sum_{nm} S_{\sigma nm}(E) \phi_n(\boldsymbol{r}) \phi_m^{*}(\boldsymbol{r}'). \tag{3}$$

We may consider $M_{\sigma}^{(I)}(\boldsymbol{r}, \boldsymbol{r}')$ as a nonlocal potential, from which we may obtain the spectral moment matrices by computing the matrix elements:

$$M_{\sigma nm}^{(I)} = \int d^3r d^3r' M_{\sigma}^{(I)}(\boldsymbol{r}, \boldsymbol{r}') \phi_n^{*}(\boldsymbol{r}) \phi_m(\boldsymbol{r}'). \tag{4}$$

According to our arguments above, the nonlocal potentials $M_\sigma^{(I)}(\boldsymbol{r},\boldsymbol{r}')$ are unique functionals of the electron density.

In KS-DFT, the total energy functional is split into the kinetic energy, the Hartree energy, and the exchange-correlation energy [2]. The kinetic energy is computed from the KS wave functions, the Hartree energy is computed from the charge density, and for the exchange-correlation energy one often uses analytical expressions in terms of the charge density, which have been derived for the uniform electron gas [25]. Similarly, the potentials $M_\sigma^{(I)}(\boldsymbol{r},\boldsymbol{r}')$ ($I = 1, 2, 3$ if we use the first four moments) contain contributions from the kinetic energy and from the Hartree term. In the following section, we show that these contributions may be identified and separated from a remainder, which thus plays a similar role in MFbS-DFT like the exchange-correlation potential does in KS-DFT. We expect that useful expressions for this remainder can be found by evaluating it for the uniform electron gas.

B. Explicit expressions for the moments

We consider the Hamiltonian

$$H = \sum_{\sigma nm} T_{nm} c_{\sigma n}^\dagger c_{\sigma m} + \frac{1}{2} \sum_{\sigma\sigma' nmn'm'} V_{nmn'm'} c_{\sigma n}^\dagger c_{\sigma' m}^\dagger c_{\sigma' m'} c_{\sigma n'}, \tag{5}$$

where

$$T_{nm} = \int d^3 r \phi_n^*(\boldsymbol{r}) \left[-\frac{1}{2}\Delta + V(\boldsymbol{r}) \right] \phi_m(\boldsymbol{r}) \tag{6}$$

and

$$V_{nmn'm'} = \int d^3 r_1 d^3 r_2 \frac{\phi_n^*(\boldsymbol{r}_1)\phi_m^*(\boldsymbol{r}_2)\phi_{m'}(\boldsymbol{r}_2)\phi_{n'}(\boldsymbol{r}_1)}{|\boldsymbol{r}_1 - \boldsymbol{r}_2|}, \tag{7}$$

and $V(\boldsymbol{r})$ is the lattice potential. Note that in the entire Sec. II B, we use the Hartree atomic units for notational convenience.

Many-body approaches such as LDA+DMFT often take into account the Coulomb matrix element $V_{nmn'm'}$ only when all orbitals, i.e., n, m, n', and m', describe the same crystal lattice site. In the simplest approximation, $V_{nmn'm'}$ is described by a single parameter, the so-called Hubbard U. Components of $V_{nmn'm'}$ that are neglected hereby are of course partly treated in LDA+DMFT, because the lattice potential $V(\boldsymbol{r})$ is replaced by the KS potential in this case. Therefore the Hubbard U only describes the Coulomb interaction from strong localization of electrons. These effects are underestimated by KS-DFT and become important when U approaches or exceeds the bandwidth. In contrast, we do not restrict $V_{nmn'm'}$ at this point, i.e., both local and nonlocal contributions are described by it in MFbSDFT and $V(\boldsymbol{r})$ is the pure lattice potential without exchange-correlation terms.

The zeroth moment is given by

$$M_{\sigma nm}^{(0)} = \langle [c_{\sigma n}, c_{\sigma m}^\dagger]_+ \rangle = \delta_{nm}, \tag{8}$$

where $[\dots]_+$ denotes the anticommutator, and the first moment evaluates to

$$M_{\sigma nm}^{(1)} = \langle [[c_{\sigma n}, H]_-, c_{\sigma m}^\dagger]_+ \rangle = T_{nm} + \sum_{n'm'\sigma'} V_{nn'mm'} \langle c_{\sigma' n'}^\dagger c_{\sigma' m'} \rangle - \sum_{n'm'} V_{nn'm'm} \langle c_{\sigma n'}^\dagger c_{\sigma m'} \rangle. \tag{9}$$

Defining the Hartree potential by

$$V^{\mathrm{H}}(\boldsymbol{r}) = \sum_{\sigma' n'm'} \int d^3 r_2 \frac{\phi_{n'}^*(\boldsymbol{r}_2)\phi_{m'}(\boldsymbol{r}_2)}{|\boldsymbol{r} - \boldsymbol{r}_2|} \langle c_{\sigma' n'}^\dagger c_{\sigma' m'} \rangle \tag{10}$$

and the nonlocal exchange potential by

$$V_\sigma^{\mathrm{X}}(\boldsymbol{r}_1, \boldsymbol{r}_2) = -\sum_{n'm'} \frac{\phi_{n'}^*(\boldsymbol{r}_2)\phi_{m'}(\boldsymbol{r}_1)}{|\boldsymbol{r}_1 - \boldsymbol{r}_2|} \langle c_{\sigma n'}^\dagger c_{\sigma m'} \rangle, \tag{11}$$

we may write the first moment as

$$M_{\sigma nm}^{(1)} = T_{nm} + V_{nm}^{\mathrm{H}} + V_{\sigma nm}^{\mathrm{X}} = \mathcal{M}_{\sigma nm}^{\mathrm{HF}}, \tag{12}$$

where V_{nm}^{H} and $V_{\sigma nm}^{\mathrm{X}}$ are the matrix elements of the Hartree potential and of the nonlocal exchange potential, respectively. Thus one obtains a method of Hartree-Fock (HF) type if one considers only the first two moments. It differs from the exact Hartree-Fock method by the self-interaction error (SIE) [26] (see also Sec. VII for a brief discussion of SIE from the perspective of MFbSDFT). Therefore we introduced the alternative label $\mathcal{M}_{\sigma nm}^{\mathrm{HF}}$ for the first moment, which expresses concisely what this first moment contains. Instead of using the nonlocal exchange potential Eq. (11), one may use the local exchange potential [2]

$$V_\sigma^{\mathrm{locX}}(\boldsymbol{r}) = \frac{\partial}{\partial n(\boldsymbol{r})} [n(\boldsymbol{r}) \epsilon^{\mathrm{X}}(n(\boldsymbol{r}))], \tag{13}$$

where

$$n(\boldsymbol{r}) = \sum_{\sigma nm} \phi_n^*(\boldsymbol{r})\phi_m(\boldsymbol{r}) \langle c_{\sigma n}^\dagger c_{\sigma m} \rangle \tag{14}$$

is the electron density at position $\boldsymbol{r}$ and $\epsilon^{\mathrm{X}}(n(\boldsymbol{r}))$ is the exchange energy density for electron density $n(\boldsymbol{r})$. The local potential Eq. (13) has the advantage that it is computationally very cheap to evaluate in contrast to the nonlocal version Eq. (11). However, hybrid density functionals, which admix exact exchange, are often more precise than density functionals that use only the local approximation Eq. (13). Fortunately, one may reduce the computational burden of exact exchange by screening the Coulomb potential [27]. In the numerical calculations in this work we will use only the local expression Eq. (13), but similar to KS-DFT, we expect that the precision of the MFbSDFT approach can be increased by avoiding the approximation of nonlocal potentials by local potentials. We leave it for future work to explore how the MFbSDFT approach may be combined with nonlocal potentials.

In Ref. [17], we explain that for independent electrons the spectral moment matrices commute, i.e.,

$$\left[\boldsymbol{M}_\sigma^{(I)}, \boldsymbol{M}_\sigma^{(J)} \right]_- = 0 \tag{15}$$

for all I and J, and that the eigenvalues of the spectral moment matrix $\boldsymbol{M}_\sigma^{(I)}$ are simply the eigenvalues of the single-particle

Hamiltonian raised to the Ith power, i.e., $(E_{\sigma n})^I$. For correlated electrons this is not the case [17]. However, we may expect that the moment $\boldsymbol{M}_\sigma^{(I)}$ contains a term $[\boldsymbol{\mathcal{M}}_\sigma^{\mathrm{HF}}]^I$, because there may be cases where Hartree-Fock provides an excellent description because correlation effects are small, and these special cases have to be accommodated by the general theory. We may therefore expect that the second moment should contain a term

$$\begin{aligned}\boldsymbol{\mathcal{M}}_\sigma^{\mathrm{HF}}\boldsymbol{\mathcal{M}}_\sigma^{\mathrm{HF}} = {}& \boldsymbol{T}\boldsymbol{T} + \boldsymbol{T}\boldsymbol{V}^{\mathrm{H}} + \boldsymbol{T}\boldsymbol{V}_\sigma^{\mathrm{X}} + \boldsymbol{V}^{\mathrm{H}}\boldsymbol{T} + \boldsymbol{V}^{\mathrm{H}}\boldsymbol{V}^{\mathrm{H}} \\ & + \boldsymbol{V}^{\mathrm{H}}\boldsymbol{V}_\sigma^{\mathrm{X}} + \boldsymbol{V}_\sigma^{\mathrm{X}}\boldsymbol{T} + \boldsymbol{V}_\sigma^{\mathrm{X}}\boldsymbol{V}^{\mathrm{H}} + \boldsymbol{V}_\sigma^{\mathrm{X}}\boldsymbol{V}_\sigma^{\mathrm{X}}, \end{aligned} \tag{16}$$

which is indeed what we find. We may use this observation to split the second moment into the anticipated part $\boldsymbol{\mathcal{M}}_\sigma^{\mathrm{HF}}\boldsymbol{\mathcal{M}}_\sigma^{\mathrm{HF}}$ plus additional new terms, which we denote by $\boldsymbol{M}_\sigma^{(2+)}$, i.e.,

$$\boldsymbol{M}_\sigma^{(2)} = \boldsymbol{\mathcal{M}}_\sigma^{\mathrm{HF}}\boldsymbol{\mathcal{M}}_\sigma^{\mathrm{HF}} + \boldsymbol{M}_\sigma^{(2+)}. \tag{17}$$

In contrast to the single-band Hubbard model with on-site Coulomb interaction, where higher-order correlation functions appear in the third moment and in the higher moments, already the second moment $\boldsymbol{M}_\sigma^{(2)}$ of the many-band case with the full Coulomb interaction contains the higher-order correlation function $\langle c_{\sigma n}^\dagger c_{\sigma' m}^\dagger c_{\sigma n'} c_{\sigma' m'}\rangle$. In order to identify the terms $\boldsymbol{V}^{\mathrm{H}}\boldsymbol{V}^{\mathrm{H}}$, $\boldsymbol{V}^{\mathrm{H}}\boldsymbol{V}_\sigma^{\mathrm{X}}$, $\boldsymbol{V}_\sigma^{\mathrm{X}}\boldsymbol{V}^{\mathrm{H}}$, and $\boldsymbol{V}_\sigma^{\mathrm{X}}\boldsymbol{V}_\sigma^{\mathrm{X}}$ predicted by Eq. (16), we need to evaluate $\langle c_{\sigma n}^\dagger c_{\sigma' m}^\dagger c_{\sigma n'} c_{\sigma' m'}\rangle$ in perturbation theory. In contrast, the terms $\boldsymbol{T}\boldsymbol{V}^{\mathrm{H}}$, $\boldsymbol{T}\boldsymbol{V}_\sigma^{\mathrm{X}}$, $\boldsymbol{V}^{\mathrm{H}}\boldsymbol{T}$, and $\boldsymbol{V}_\sigma^{\mathrm{X}}\boldsymbol{T}$ can be identified without using perturbation theory, because they appear with the correlation function $\langle c_{\sigma' m}^\dagger c_{\sigma' m'}\rangle$. The term $\boldsymbol{T}\boldsymbol{T}$ appears even without any correlation function. Therefore we define

$$\begin{aligned}\langle\langle c_{\sigma n}^\dagger c_{\sigma' m}^\dagger c_{\sigma n'} c_{\sigma' m'}\rangle\rangle = {}& \langle c_{\sigma n}^\dagger c_{\sigma' m}^\dagger c_{\sigma n'} c_{\sigma' m'}\rangle \\ & - \langle c_{\sigma n}^\dagger c_{\sigma' m'}\rangle\langle c_{\sigma' m}^\dagger c_{\sigma n'}\rangle \\ & + \langle c_{\sigma n}^\dagger c_{\sigma n'}\rangle\langle c_{\sigma' m}^\dagger c_{\sigma' m'}\rangle. \end{aligned} \tag{18}$$

The idea behind Eq. (18) is that the diagrammatic expression of $\langle c_{\sigma n}^\dagger c_{\sigma' m}^\dagger c_{\sigma n'} c_{\sigma' m'}\rangle$ as obtained within perturbation theory contains terms that may be written as $\langle c_{\sigma n}^\dagger c_{\sigma' m'}\rangle\langle c_{\sigma' m}^\dagger c_{\sigma n'}\rangle$ and $-\langle c_{\sigma n}^\dagger c_{\sigma n'}\rangle\langle c_{\sigma' m}^\dagger c_{\sigma' m'}\rangle$. Since these latter two terms occur sometimes in $\boldsymbol{\mathcal{M}}_\sigma^{\mathrm{HF}}\boldsymbol{\mathcal{M}}_\sigma^{\mathrm{HF}}$ we introduce the notation of Eq. (18) in order to split $\boldsymbol{M}_\sigma^{(2)}$ into $\boldsymbol{\mathcal{M}}_\sigma^{\mathrm{HF}}\boldsymbol{\mathcal{M}}_\sigma^{\mathrm{HF}}$ and $\boldsymbol{M}_\sigma^{(2+)}$. Using this notation we may write $\boldsymbol{M}_\sigma^{(2+)}$ as a sum of 17 terms:

$$M_{nm}^{(2+,1)} = \sum_{n'm'tt'\sigma'} V_{nn'tt'} V_{t't m'm} \langle c_{\sigma' n'}^\dagger c_{\sigma' m'}\rangle, \tag{19}$$

which is spin-independent,

$$M_{\sigma nm}^{(2+,2)} = -\sum_{n'm'tt'} V_{nn'tt'} V_{tt'm'm} \langle c_{\sigma n'}^\dagger c_{\sigma m'}\rangle, \tag{20}$$

$$M_{nm}^{(2+,3)} = -\sum_{n'm'tt'z\sigma'} V_{nn'zt'} V_{tzm'm} \langle\langle c_{\sigma' n'}^\dagger c_{\sigma' t}^\dagger c_{\sigma' t'} c_{\sigma' m'}\rangle\rangle, \tag{21}$$

which does not depend on the spin,

$$M_{\sigma nm}^{(2+,4)} = -\sum_{n'm'tt'z} V_{nn't't} V_{tm'zm} \langle\langle c_{\sigma n'}^\dagger c_{\sigma m'}^\dagger c_{\sigma t'} c_{\sigma z}\rangle\rangle, \tag{22}$$

$$M_{\sigma nm}^{(2+,5)} = \sum_{n'm'tt'z} V_{nn'tt'} V_{tm'zm} \langle\langle c_{\sigma n'}^\dagger c_{\sigma m'}^\dagger c_{\sigma t'} c_{\sigma z}\rangle\rangle, \tag{23}$$

$$M_{\sigma nm}^{(2+,6)} = \sum_{n'm'tt'z} V_{nn'tt'} V_{zm'n'm} \langle c_{\sigma z}^\dagger c_{\sigma m'}^\dagger c_{\sigma t} c_{\sigma t'}\rangle, \tag{24}$$

$$M_{\sigma nm}^{(2+,7)} = \sum_{n'm'tt'z} V_{nn'tz} V_{m'zt'm} \langle\langle c_{\sigma n'}^\dagger c_{\sigma m'}^\dagger c_{\sigma t} c_{\sigma t'}\rangle\rangle, \tag{25}$$

$$M_{\sigma nm}^{(2+,8)} = -\sum_{n'm'tt'z} V_{nn't't'} V_{zm'n'm} \langle c_{\sigma m'}^\dagger c_{-\sigma z}^\dagger c_{\sigma t} c_{-\sigma t'}\rangle, \tag{26}$$

$$M_{\sigma nm}^{(2+,9)} = -\sum_{n'm'tt'z} V_{nn't't'} V_{m'tzm} \langle\langle c_{\sigma n'}^\dagger c_{-\sigma m'}^\dagger c_{\sigma t'} c_{-\sigma z}\rangle\rangle, \tag{27}$$

$$M_{\sigma nm}^{(2+,10)} = -\sum_{n'm'tt'z} V_{nn't't'} V_{m'tzm} \langle\langle c_{\sigma m'}^\dagger c_{-\sigma n'}^\dagger c_{\sigma z} c_{-\sigma t'}\rangle\rangle, \tag{28}$$

$$M_{\sigma nm}^{(2+,11)} = \sum_{n'm'tt'z} V_{nn't't'} V_{tm'zm} \langle\langle c_{\sigma m'}^\dagger c_{-\sigma n'}^\dagger c_{\sigma z} c_{-\sigma t'}\rangle\rangle, \tag{29}$$

$$M_{\sigma nm}^{(2+,12)} = \sum_{n'm'tt'z} V_{nn't't'} V_{t'm'zm} \langle c_{\sigma m'}^\dagger c_{-\sigma n'}^\dagger c_{\sigma t} c_{-\sigma z}\rangle, \tag{30}$$

$$M_{\sigma nm}^{(2+,13)} = \sum_{n'm'tt'z} V_{nn't't'} V_{m't'zm} \langle\langle c_{\sigma n'}^\dagger c_{-\sigma m'}^\dagger c_{\sigma t} c_{-\sigma z}\rangle\rangle, \tag{31}$$

$$M_{nm}^{(2+,14)} = -\sum_{\sigma' n'm'tt'z} V_{nn't't'} V_{m'tzm} \langle c_{\sigma' m'}^\dagger c_{\sigma' t'}\rangle\langle c_{\sigma' n'}^\dagger c_{\sigma' z}\rangle, \tag{32}$$

which is spin-independent,

$$M_{\sigma nm}^{(2+,15)} = -\sum_{n'm'tt'z} V_{nn't't'} V_{t'm'zm} \langle c_{\sigma m'}^\dagger c_{\sigma t}\rangle\langle c_{\sigma n'}^\dagger c_{\sigma z}\rangle, \tag{33}$$

$$M_{\sigma nm}^{(2+,16)} = \sum_{n'm'tt'z} V_{nn't't'} V_{tm'zm} \langle c_{\sigma m'}^\dagger c_{\sigma t'}\rangle\langle c_{\sigma n'}^\dagger c_{\sigma z}\rangle, \tag{34}$$

and

$$M_{\sigma nm}^{(2+,17)} = \sum_{n'm'tt'z} V_{nn't't'} V_{m't'zm} \langle c_{\sigma m'}^\dagger c_{\sigma t}\rangle\langle c_{\sigma n'}^\dagger c_{\sigma z}\rangle. \tag{35}$$

In order to evaluate the contributions to $\boldsymbol{M}^{(2+)}$ in a way similar to Eq. (13), we suggest to consider the contractions

$$\mathcal{C}_\sigma^{(2+,j)} = \sum_{nm} M_{\sigma nm}^{(2+,j)} \langle c_{\sigma n}^\dagger c_{\sigma m}\rangle \tag{36}$$

and to compute them for the uniform electron gas as a function of electron density. Similarly to Eq. (13), we assume that we may derive local potentials

$$\mathcal{V}_\sigma^{(2+,j)}(\boldsymbol{r}) = \frac{\partial}{\partial n(\boldsymbol{r})}\left[\mathcal{C}_\sigma^{(2+,j)}\right] \tag{37}$$

from these contractions and compute the moments from these local potentials:

$$M_{\sigma nm}^{(2+,j)} = \int d^3r \mathcal{V}_\sigma^{(2+,j)}(\boldsymbol{r}) \phi_n^*(\boldsymbol{r}) \phi_m(\boldsymbol{r}). \tag{38}$$

Many popular exchange-correlation potentials are constructed with the help of Green's function Monte Carlo simulations of the energy of the uniform electron gas [25,28], because the universality of the exchange correlation potential implies that it may be constructed from a uniform system. However, Green's function Monte Carlo data are not yet available for our expressions Eq. (19) through Eq. (35). On the other hand, diagrammatic perturbation theory has been used to derive expressions for the energy of the uniform electron gas in the limit of low and high density and these results are considered in the construction of exchange correlation potentials as well [25,29]. For the purpose of demonstrating the feasibility of the MFbSDFT approach, it is sufficient to find simple approximate expressions for the contractions Eq. (36). Therefore we

evaluate these contractions for the uniform electron gas using perturbation theory in Appendix B. We leave it for future work to find accurate analytic representations of the contractions of Eq. (19) through Eq. (35) based on techniques such as Green's function Monte Carlo simulations and diagrammatic expansions for the high-density limit.

Similar to Eq. (17), one may anticipate that the third moment may be decomposed as

$$\boldsymbol{M}_\sigma^{(3)} = \boldsymbol{\mathcal{M}}_\sigma^{\mathrm{HF}} \boldsymbol{\mathcal{M}}_\sigma^{\mathrm{HF}} \boldsymbol{\mathcal{M}}_\sigma^{\mathrm{HF}} + \boldsymbol{M}_\sigma^{(3+)}, \tag{39}$$

where

$$\begin{aligned}
&\boldsymbol{\mathcal{M}}_\sigma^{\mathrm{HF}} \boldsymbol{\mathcal{M}}_\sigma^{\mathrm{HF}} \boldsymbol{\mathcal{M}}_\sigma^{\mathrm{HF}} \\
&= \boldsymbol{T}\boldsymbol{T}\boldsymbol{T} + \boldsymbol{T}\boldsymbol{T}\boldsymbol{V}^{\mathrm{H}} + \boldsymbol{T}\boldsymbol{T}\boldsymbol{V}_\sigma^{\mathrm{X}} \\
&\quad + \boldsymbol{T}\boldsymbol{V}^{\mathrm{H}}\boldsymbol{T} + \boldsymbol{T}\boldsymbol{V}^{\mathrm{H}}\boldsymbol{V}^{\mathrm{H}} + \boldsymbol{T}\boldsymbol{V}^{\mathrm{H}}\boldsymbol{V}_\sigma^{\mathrm{X}} \\
&\quad + \boldsymbol{T}\boldsymbol{V}_\sigma^{\mathrm{X}}\boldsymbol{T} + \boldsymbol{V}^{\mathrm{H}}\boldsymbol{T}\boldsymbol{V}_\sigma^{\mathrm{X}}\boldsymbol{V}^{\mathrm{H}} + \boldsymbol{V}^{\mathrm{H}}\boldsymbol{T}\boldsymbol{V}_\sigma^{\mathrm{X}}\boldsymbol{V}_\sigma^{\mathrm{X}} \\
&\quad + \boldsymbol{V}^{\mathrm{H}}\boldsymbol{T}\boldsymbol{T} + \boldsymbol{V}^{\mathrm{H}}\boldsymbol{T}\boldsymbol{V}^{\mathrm{H}} + \boldsymbol{V}^{\mathrm{H}}\boldsymbol{T}\boldsymbol{V}_\sigma^{\mathrm{X}} \\
&\quad + \boldsymbol{V}^{\mathrm{H}}\boldsymbol{V}^{\mathrm{H}}\boldsymbol{T} + \boldsymbol{V}^{\mathrm{H}}\boldsymbol{V}^{\mathrm{H}}\boldsymbol{V}^{\mathrm{H}} + \boldsymbol{V}^{\mathrm{H}}\boldsymbol{V}^{\mathrm{H}}\boldsymbol{V}_\sigma^{\mathrm{X}} \\
&\quad + \boldsymbol{V}^{\mathrm{H}}\boldsymbol{V}_\sigma^{\mathrm{X}}\boldsymbol{T} + \boldsymbol{V}^{\mathrm{H}}\boldsymbol{V}_\sigma^{\mathrm{X}}\boldsymbol{V}^{\mathrm{H}} + \boldsymbol{V}^{\mathrm{H}}\boldsymbol{V}_\sigma^{\mathrm{X}}\boldsymbol{V}_\sigma^{\mathrm{X}} \\
&\quad + \boldsymbol{V}_\sigma^{\mathrm{X}}\boldsymbol{T}\boldsymbol{T} + \boldsymbol{V}_\sigma^{\mathrm{X}}\boldsymbol{T}\boldsymbol{V}^{\mathrm{H}} + \boldsymbol{V}_\sigma^{\mathrm{X}}\boldsymbol{T}\boldsymbol{V}_\sigma^{\mathrm{X}} \\
&\quad + \boldsymbol{V}_\sigma^{\mathrm{X}}\boldsymbol{V}^{\mathrm{H}}\boldsymbol{T} + \boldsymbol{V}_\sigma^{\mathrm{X}}\boldsymbol{V}^{\mathrm{H}}\boldsymbol{V}^{\mathrm{H}} + \boldsymbol{V}_\sigma^{\mathrm{X}}\boldsymbol{V}^{\mathrm{H}}\boldsymbol{V}_\sigma^{\mathrm{X}} \\
&\quad + \boldsymbol{V}_\sigma^{\mathrm{X}}\boldsymbol{V}_\sigma^{\mathrm{X}}\boldsymbol{T} + \boldsymbol{V}_\sigma^{\mathrm{X}}\boldsymbol{V}_\sigma^{\mathrm{X}}\boldsymbol{V}^{\mathrm{H}} + \boldsymbol{V}_\sigma^{\mathrm{X}}\boldsymbol{V}_\sigma^{\mathrm{X}}\boldsymbol{V}_\sigma^{\mathrm{X}},
\end{aligned} \tag{40}$$

which is indeed what we find: To identify $\boldsymbol{T}\boldsymbol{T}\boldsymbol{T}$ in $\boldsymbol{M}_\sigma^{(3)}$ one needs to check the terms without correlation functions. To find the terms that contain two factors of the matrix $\boldsymbol{T}$, i.e., the terms $\boldsymbol{T}\boldsymbol{T}\boldsymbol{V}^{\mathrm{H}}$, $\boldsymbol{T}\boldsymbol{V}^{\mathrm{H}}\boldsymbol{T}$, $\boldsymbol{V}^{\mathrm{H}}\boldsymbol{T}\boldsymbol{T}$, $\boldsymbol{T}\boldsymbol{T}\boldsymbol{V}^{\mathrm{X}}$, $\boldsymbol{T}\boldsymbol{V}^{\mathrm{X}}\boldsymbol{T}$, and $\boldsymbol{V}^{\mathrm{X}}\boldsymbol{T}\boldsymbol{T}$, one needs to look out for the contributions to $\boldsymbol{M}_\sigma^{(3)}$ that contain the correlation function $\langle c^\dagger_{\sigma' m} c_{\sigma' m'}\rangle$. To track down the terms that contain a single factor of the matrix $\boldsymbol{T}$, i.e., the terms $\boldsymbol{T}\boldsymbol{V}^{\mathrm{H}}\boldsymbol{V}^{\mathrm{H}}$, $\boldsymbol{V}^{\mathrm{H}}\boldsymbol{T}\boldsymbol{V}^{\mathrm{H}}$, $\boldsymbol{V}^{\mathrm{H}}\boldsymbol{V}^{\mathrm{H}}\boldsymbol{T}$, $\boldsymbol{T}\boldsymbol{V}^{\mathrm{H}}\boldsymbol{V}^{\mathrm{X}}$, $\boldsymbol{V}^{\mathrm{H}}\boldsymbol{T}\boldsymbol{V}^{\mathrm{X}}$, $\boldsymbol{V}^{\mathrm{H}}\boldsymbol{V}^{\mathrm{X}}\boldsymbol{T}$, $\boldsymbol{T}\boldsymbol{V}^{\mathrm{X}}\boldsymbol{V}^{\mathrm{H}}$, $\boldsymbol{V}^{\mathrm{X}}\boldsymbol{T}\boldsymbol{V}^{\mathrm{H}}$, $\boldsymbol{V}^{\mathrm{X}}\boldsymbol{V}^{\mathrm{H}}\boldsymbol{T}$, $\boldsymbol{T}\boldsymbol{V}^{\mathrm{X}}\boldsymbol{V}^{\mathrm{X}}$, $\boldsymbol{V}^{\mathrm{X}}\boldsymbol{T}\boldsymbol{V}^{\mathrm{X}}$, and $\boldsymbol{V}^{\mathrm{X}}\boldsymbol{V}^{\mathrm{X}}\boldsymbol{T}$, one needs to find the contributions to $\boldsymbol{M}_\sigma^{(3)}$ that contain the correlation function $\langle c^\dagger_{\sigma m} c^\dagger_{\sigma' m'} c_{\sigma n} c_{\sigma' n'}\rangle$ and one has to evaluate this correlation function in perturbation theory. In order to identify all those terms in Eq. (40) that do not contain the matrix $\boldsymbol{T}$, i.e., the terms $\boldsymbol{V}^{\mathrm{H}}\boldsymbol{V}^{\mathrm{H}}\boldsymbol{V}^{\mathrm{H}}$, $\boldsymbol{V}^{\mathrm{X}}\boldsymbol{V}^{\mathrm{H}}\boldsymbol{V}^{\mathrm{H}}$, $\boldsymbol{V}^{\mathrm{H}}\boldsymbol{V}^{\mathrm{X}}\boldsymbol{V}^{\mathrm{H}}$, $\boldsymbol{V}^{\mathrm{H}}\boldsymbol{V}^{\mathrm{H}}\boldsymbol{V}^{\mathrm{X}}$, $\boldsymbol{V}^{\mathrm{H}}\boldsymbol{V}^{\mathrm{X}}\boldsymbol{V}^{\mathrm{X}}$, $\boldsymbol{V}^{\mathrm{X}}\boldsymbol{V}^{\mathrm{H}}\boldsymbol{V}^{\mathrm{X}}$, $\boldsymbol{V}^{\mathrm{X}}\boldsymbol{V}^{\mathrm{X}}\boldsymbol{V}^{\mathrm{H}}$, and $\boldsymbol{V}^{\mathrm{X}}\boldsymbol{V}^{\mathrm{X}}\boldsymbol{V}^{\mathrm{X}}$, one needs to check the expressions that contain the correlation function $\langle c^\dagger_{\sigma m} c^\dagger_{\sigma' m'} c^\dagger_{\sigma'' t'} c_{\sigma n} c_{\sigma' n'} c_{\sigma'' t'}\rangle$ and one has to evaluate this correlation function in perturbation theory.

When one evaluates the correlator $\langle c^\dagger_{\sigma n} c^\dagger_{\sigma' m} c_{\sigma n'} c_{\sigma' m'}\rangle$ in perturbation theory in order to extract the terms discussed above, e.g., $\boldsymbol{V}^{\mathrm{H}}\boldsymbol{V}^{\mathrm{H}}\boldsymbol{T}$, one may use Eq. (18) like for the second moment. This procedure generates a group of terms in $\boldsymbol{M}_\sigma^{(3+)}$ that contain $\langle\langle c^\dagger_{\sigma n} c^\dagger_{\sigma' m} c_{\sigma n'} c_{\sigma' m'}\rangle\rangle$. Similarly, it is convenient to define

$$\begin{aligned}
&\langle\langle c^\dagger_{\sigma m} c^\dagger_{\sigma' m'} c^\dagger_{\sigma'' t} c_{\sigma n} c_{\sigma' n'} c_{\sigma'' t'}\rangle\rangle \\
&\quad = \langle c^\dagger_{\sigma m} c^\dagger_{\sigma' m'} c^\dagger_{\sigma'' t} c_{\sigma n} c_{\sigma' n'} c_{\sigma'' t'}\rangle \\
&\qquad - \langle c^\dagger_{\sigma m} c_{\sigma n}\rangle \langle c^\dagger_{\sigma' m'} c^\dagger_{\sigma'' t} c_{\sigma' n'} c_{\sigma'' t'}\rangle \\
&\qquad + \langle c^\dagger_{\sigma m} c_{\sigma' n'}\rangle \langle c^\dagger_{\sigma' m'} c^\dagger_{\sigma'' t} c_{\sigma n} c_{\sigma'' t'}\rangle \\
&\qquad - \langle c^\dagger_{\sigma m} c_{\sigma'' t'}\rangle \langle c^\dagger_{\sigma' m'} c^\dagger_{\sigma'' t} c_{\sigma n} c_{\sigma' n'}\rangle
\end{aligned} \tag{41}$$

and to use Eq. (18) in order to replace the correlators of the type $\langle c^\dagger_{\sigma' m'} c^\dagger_{\sigma'' t} c_{\sigma' n'} c_{\sigma'' t'}\rangle$ on the right-hand side of Eq. (41) by $\langle\langle c^\dagger_{\sigma' m'} c^\dagger_{\sigma'' t} c_{\sigma' n'} c_{\sigma'' t'}\rangle\rangle$ and the simpler correlators $\langle c^\dagger_{\sigma' m'} c_{\sigma' n'}\rangle$. When we use this procedure to express $\langle c^\dagger_{\sigma m} c^\dagger_{\sigma' m'} c^\dagger_{\sigma'' t} c_{\sigma n} c_{\sigma' n'} c_{\sigma'' t'}\rangle$ in terms of the correlators $\langle c^\dagger_{\sigma' m'} c_{\sigma' n'}\rangle$ and thereby extract the terms discussed above, e.g., $\boldsymbol{V}^{\mathrm{H}}\boldsymbol{V}^{\mathrm{H}}\boldsymbol{V}^{\mathrm{H}}$, we generate additional groups of terms in $\boldsymbol{M}_\sigma^{(3+)}$, which contain $\langle\langle c^\dagger_{\sigma' m'} c^\dagger_{\sigma'' t} c_{\sigma' n'} c_{\sigma'' t'}\rangle\rangle$ or $\langle\langle c^\dagger_{\sigma m} c^\dagger_{\sigma' m'} c^\dagger_{\sigma'' t} c_{\sigma n} c_{\sigma' n'} c_{\sigma'' t'}\rangle\rangle$.

The remaining contributions to $\boldsymbol{M}_\sigma^{(3+)}$ may be split into groups of formally similar expressions. The first group of two terms in $\boldsymbol{M}_\sigma^{(3+)}$ contains two matrices $\boldsymbol{T}$ and the correlation function $\langle c^\dagger_{\sigma' m} c_{\sigma' m'}\rangle$:

$$M_{nm}^{(3+,1)} = \sum_{n' t' \sigma'} V_{nn' t' t} T_{tm} S_{\sigma' t' n'}, \tag{42}$$

which is spin-independent, and

$$M_{\sigma nm}^{(3+,2)} = -\sum_{n' t'} V_{nn' t' t} T_{tm} S_{\sigma t' n'}, \tag{43}$$

where

$$S_{\sigma' t' n'} = \sum_{m'} [T_{t' m'} \langle c^\dagger_{\sigma' n'} c_{\sigma' m'}\rangle - \langle c^\dagger_{\sigma' m'} c_{\sigma' t'}\rangle T_{m' n'}] \tag{44}$$

is the commutator between the matrix $\boldsymbol{T}$ and the density matrix.

It is desirable to rewrite Eq. (42) in a form that permits a numerically efficient evaluation of this term, because the direct computation of Eq. (42) will often be numerically demanding due to the four indices of the Coulomb matrix element. We may exploit that the indices t' and n' couple to the Coulomb matrix element in a way that allows us to identify the density matrix. Therefore we may define

$$\mathcal{N}(\boldsymbol{r}) = \sum_{n' t' \sigma'} \phi^*_{n'}(\boldsymbol{r}) \phi_{t'}(\boldsymbol{r}) S_{\sigma' t' n'}, \tag{45}$$

from which we compute the Hartree-type integral

$$\mathcal{F}(\boldsymbol{r}) = \int d^3 r_2 \frac{\mathcal{N}(\boldsymbol{r}_2)}{|\boldsymbol{r} - \boldsymbol{r}_2|}. \tag{46}$$

Equation (42) may now be written as

$$M_{nm}^{(3+,1)} = \sum_t \mathcal{F}_{nt} T_{tm}, \tag{47}$$

where $\mathcal{F}_{nt}$ are the matrix elements of the Hartree-type potential $\mathcal{F}(\boldsymbol{r})$.

Similarly, in order to evaluate Eq. (43), we may exploit that the indices t' and n' couple to the Coulomb matrix element in a way that allows us to identify a nonlocal potential. Therefore we may define

$$\mathcal{L}_\sigma(\boldsymbol{r}_1, \boldsymbol{r}_2) = \sum_{n' t'} \frac{\phi^*_{n'}(\boldsymbol{r}_1) \phi_{t'}(\boldsymbol{r}_2)}{|\boldsymbol{r}_1 - \boldsymbol{r}_2|} S_{\sigma' t' n'}. \tag{48}$$

Equation (43) may now be written as

$$M_{\sigma nm}^{(3+,2)} = -\sum_t \mathcal{L}_{\sigma nt} T_{tm}, \tag{49}$$

where $\mathcal{L}_{\sigma nt}$ are the matrix elements of the nonlocal Fock-type potential $\mathcal{L}_\sigma(\boldsymbol{r}_1, \boldsymbol{r}_2)$.

The next group of two terms in $\boldsymbol{M}_{\sigma}^{(3+)}$ does not contain the matrix $\boldsymbol{T}$, but it contains the correlation function $\langle c^{\dagger}_{\sigma' m} c_{\sigma' m'} \rangle$:

$$M^{(3+,3)}_{nm} = \sum_{\sigma' n' t t'} \sum_{z z' m'} V_{nn' t t'} V_{t t' z z'} V_{z' z m' m} \langle c^{\dagger}_{\sigma' n'} c_{\sigma' m'} \rangle, \tag{50}$$

which does not depend on the spin, and

$$M^{(3+,4)}_{\sigma nm} = -\sum_{n' t t'} \sum_{z z' m'} V_{nn' t t'} V_{t t' z' z} V_{z' z m' m} \langle c^{\dagger}_{\sigma n'} c_{\sigma m'} \rangle. \tag{51}$$

In Appendix A, we show that the sum of Eqs. (50) and (51) turns into the very simple result $U^3 \langle n_{-\sigma} \rangle$ in the case of the single-band Hubbard model. However, for realistic many-band systems, the direct evaluation of these expressions may be numerically demanding due to the four indices of the Coulomb matrix element. Therefore we may try to use concepts from DFT to simplify the calculations. In order to approximate these contributions by local functionals, we may use the recipe described above in Eqs. (36), (37), and (38). In Appendix C, we evaluate the corresponding contractions for the uniform electron gas.

$\boldsymbol{M}^{(3+)}$ contains several additional groups of terms that we have not discussed yet. One group of terms contains three factors of the Coulomb matrix element and the correlator $\langle c^{\dagger}_{\sigma m} c^{\dagger}_{\sigma' m'} c^{\dagger}_{\sigma'' t} c_{\sigma n} c_{\sigma' n'} c_{\sigma'' t'} \rangle$, but the indices are not connected in a way that terms such as $\boldsymbol{HHH}$ or $\boldsymbol{HXH}$ arise, which we have already discussed above. An example from this group of terms is

$$M^{(3+,5)}_{\sigma nm} = -\sum_{n' t t'} \sum_{u u'} \sum_{z z' m'} V_{nn' t t'} V_{t' m' u u'} V_{z z' m' m} \times \langle c^{\dagger}_{\sigma n'} c^{\dagger}_{\sigma z} c^{\dagger}_{\sigma z'} c_{\sigma t} c_{\sigma u} c_{\sigma u'} \rangle. \tag{52}$$

The first index t' of $V_{t' m' u u'}$ is shared with $V_{nn' t t'}$, while the second index m' of $V_{t' m' u u'}$ is shared with $V_{z z' m' m}$. The last two indices, u and u' are contracted with the correlation function $\langle c^{\dagger}_{\sigma n'} c^{\dagger}_{\sigma z} c^{\dagger}_{\sigma z'} c_{\sigma t} c_{\sigma u} c_{\sigma u'} \rangle$. In this term, it is therefore not possible to express $V_{t' m' u u'}$ through the matrices $\boldsymbol{H}$ or $\boldsymbol{X}$ when perturbation theory is used. Other terms in this group differ from Eq. (52), for example, due to different spin quantum numbers in the correlation function, e.g., $\langle c^{\dagger}_{-\sigma n'} c^{\dagger}_{\sigma z} c^{\dagger}_{\sigma z'} c_{\sigma t} c_{-\sigma u} c_{\sigma u'} \rangle$, or they differ due to different indices of the Coulomb matrix elements, e.g., $V_{n t' u u'} V_{m' n' t t'} V_{z z' m' m}$.

There is a second group of terms that contains three factors of the Coulomb matrix element as well. However, it contains the correlator $\langle c^{\dagger}_{\sigma m} c^{\dagger}_{\sigma' m'} c_{\sigma n} c_{\sigma' n'} \rangle$ instead. An example from this group of terms is

$$M^{(3+,6)}_{\sigma nm} = -\sum_{n' t t'} \sum_{z z'} \sum_{u u'} V_{nn' t t'} V_{t t' z z'} V_{z' u u' m} \times \langle c^{\dagger}_{\sigma n'} c^{\dagger}_{\sigma u} c_{\sigma z} c_{\sigma u'} \rangle. \tag{53}$$

Since $V_{t t' z z'}$ couples to the correlation function only through the index z, it cannot be expressed through the matrices $\boldsymbol{H}$ or $\boldsymbol{X}$ when perturbation theory is used. Similar to the previous group, the other members in this group differ from this example due to different spin quantum numbers in the correlation function, or due to different indices of the Coulomb matrix elements.

Another group of terms contains the matrix $\boldsymbol{T}$ once, the Coulomb matrix elements twice, and the correlation function $\langle c^{\dagger}_{\sigma m'} c_{\sigma n'} \rangle$. An example from this group of terms is

$$M^{(3+,7)}_{\sigma nm} = -\sum_{t t'} \sum_{n' m' z} V_{nn' t t'} V_{t t' z m'} T_{m' m} \langle c^{\dagger}_{\sigma n'} c_{\sigma z} \rangle. \tag{54}$$

Similar to the previous two groups, the other members in this group differ from the example of Eq. (54) due to different spin quantum numbers in the correlator, i.e., $\langle c^{\dagger}_{-\sigma n'} c_{-\sigma z} \rangle$, and due to different indices in the Coulomb matrix elements.

A similar group of terms contains the correlator $\langle c^{\dagger}_{\sigma' z'} c^{\dagger}_{\sigma u} c_{\sigma' z} c_{\sigma t'} \rangle$ instead of $\langle c^{\dagger}_{\sigma n'} c_{\sigma z} \rangle$. An example is given by

$$M^{(3+,8)}_{\sigma nm} = \sum_{t t'} \sum_{n' m' z} V_{n t m' t'} V_{z' u z t} T_{m' m} \langle c^{\dagger}_{-\sigma z'} c^{\dagger}_{\sigma u} c_{-\sigma z} c_{\sigma t'} \rangle. \tag{55}$$

III. CONSTRUCTION OF THE SPECTRAL FUNCTION FROM THE SPECTRAL MOMENTS

In Ref. [17], we have shown that the spectral function of four spectral moment matrices of size $N \times N$ may be obtained by solving $4N^2$ coupled nonlinear equations. While this approach is efficient for small N, it may become inefficient for large N. The reason may be understood from the amount of computer memory needed to store the Jacobian of the system of nonlinear equations. The size of the Jacobian scales like $16N^4$. In contrast, the size of the KS Hamiltonian matrix used in DFT codes scales like N^2 with the number N of basis functions. Therefore we describe an alternative algorithm in this section, which is more efficient than solving systems of coupled nonlinear equations when N is large. Since we discuss in Ref. [17] that finding the spectral function from noncommuting spectral matrices can be interpreted as a generalization of matrix diagonalization, it is perhaps not surprising that the new algorithm that we describe in this section uses such concepts.

In the following, we describe the algorithm to construct the spectral function from the spectral moment matrices $\boldsymbol{M}^{(1)}$, $\boldsymbol{M}^{(2)}$, and $\boldsymbol{M}^{(3)}$, where we assume that the zeroth spectral moment matrix is simply the unit matrix. Only the final result is described here, while the detailed proof is given in Appendix D. First, construct the Hermitian $N \times N$ matrix

$$\boldsymbol{M}^{(2+)} = \boldsymbol{M}^{(2)} - \boldsymbol{M}^{(1)} \boldsymbol{M}^{(1)}. \tag{56}$$

Next, diagonalize $\boldsymbol{M}^{(2+)}$:

$$\boldsymbol{M}^{(2+)} = \boldsymbol{U} \boldsymbol{D} \boldsymbol{U}^{\dagger}, \tag{57}$$

where $\boldsymbol{U}$ is a unitary matrix and $\boldsymbol{D}$ is a diagonal matrix. Using $\boldsymbol{D}$ and $\boldsymbol{U}$ construct the matrix

$$\boldsymbol{B}_1 = \boldsymbol{U} \sqrt{\boldsymbol{D}}. \tag{58}$$

Employ the inverse of its Hermitian adjoint together with the moment matrices to compute the matrix

$$\boldsymbol{B}_2 = [\boldsymbol{M}^{(3)} - \boldsymbol{M}^{(2)} \boldsymbol{M}^{(1)}] [\boldsymbol{B}_1^{\dagger}]^{-1}. \tag{59}$$

Use it to obtain the matrix

$$\boldsymbol{D}_1 = \boldsymbol{B}_1^{-1} [\boldsymbol{B}_2 - \boldsymbol{M}^{(1)} \boldsymbol{B}_1]. \tag{60}$$

Finally, take $\boldsymbol{B}_1$, $\boldsymbol{D}_1$ and the first moment matrix to construct the $2N \times 2N$ matrix

$$\boldsymbol{\mathcal{B}}^{(1)} = \begin{pmatrix} \boldsymbol{M}^{(1)} & \boldsymbol{B}_1 \\ \boldsymbol{B}_1^{\dagger} & \boldsymbol{D}_1 \end{pmatrix} \tag{61}$$

and diagonalize it:

$$\boldsymbol{\mathcal{B}}^{(1)} = \boldsymbol{\mathcal{U}}\boldsymbol{\mathcal{D}}\boldsymbol{\mathcal{U}}^{\dagger}. \tag{62}$$

The unitary matrix $\boldsymbol{\mathcal{U}}$ contains the normalized eigenvectors of $\boldsymbol{\mathcal{B}}^{(1)}$ as its columns. Compute the spectral weight of state j from

$$a_j = \sum_{i=1}^{N} \mathcal{U}_{ij}[\mathcal{U}_{ij}]^*. \tag{63}$$

Note that a_j may be smaller than one, because the summation over the index i goes only from 1 to N and not from 1 to $2N$. Therefore spectral weights smaller than 1 may occur when bands split into lower and upper Hubbard bands.

Construct the $N\times 2N$ matrix $\boldsymbol{\mathcal{V}}$ according to

$$\mathcal{V}_{ij} = \frac{\mathcal{U}_{ij}}{\sqrt{a_j}}. \tag{64}$$

Note that $i = 1, \ldots, N$, i.e., only the first N entries of the jth column of $\boldsymbol{\mathcal{U}}$ are used, while every column of $\boldsymbol{\mathcal{U}}$ has of course $2N$ entries in total.

The spectral function is given by

$$\frac{S_{ij}(E)}{\hbar} = \sum_{l=1}^{2N} a_l \mathcal{V}_{il}\mathcal{V}^*_{jl}\delta(E - E_l), \tag{65}$$

where E_l is the lth diagonal element of $\boldsymbol{\mathcal{D}}$, i.e., $E_l = \mathcal{D}_{ll}$. Here, $1 \leqslant i, j \leqslant N$, because in Eq. (64) we utilize only the first $N\times 2N$ block of the $2N\times 2N$ matrix $\boldsymbol{\mathcal{U}}$ to construct the matrix $\boldsymbol{\mathcal{V}}$.

Note that in this paper, we do not use the grand canonical Hamiltonian $\mathcal{H} = H - \mu\hat{N}$, where μ is the chemical potential, but instead we use H, because most DFT codes do not work with $\mathcal{H} = H - \mu\hat{N}$, as the chemical potential μ is typically redetermined only before the end of every iteration in the self-consistency loop to achieve matching between electronic and nuclear charge, i.e., charge neutrality. When comparing our result Eq. (65) to the literature, one therefore needs to be aware of this difference by μ in the expressions for the spectral function.

IV. CHOICE OF THE MOMENT FUNCTIONALS

In Appendix B, we have shown that

$$\mathcal{V}^{(2+)}_{\sigma}(\boldsymbol{r}) = \frac{c^{(2+)}_{\sigma}}{[r_s(\boldsymbol{r})]^2} + \cdots \tag{66}$$

and in Appendix C, we have found

$$\mathcal{V}^{(3+)}_{\sigma}(\boldsymbol{r}) = \frac{c^{(3+)}_{\sigma}}{[r_s(\boldsymbol{r})]^3} + \cdots, \tag{67}$$

where

$$r_s(\boldsymbol{r}) = \frac{1}{a_{\mathrm{B}}}\left(\frac{9\pi}{4[k_{\mathrm{F}}(\boldsymbol{r})]^3}\right)^{\frac{1}{3}} = \left(\frac{3}{4\pi n(\boldsymbol{r})}\right)^{\frac{1}{3}} \tag{68}$$

is the dimensionless density parameter. The corresponding matrix elements of the moments are obtained from these potentials according to

$$M^{(2+)}_{\sigma nm} = \int d^3r \mathcal{V}^{(2+)}_{\sigma}(\boldsymbol{r})\phi^*_n(\boldsymbol{r})\phi_m(\boldsymbol{r}) \tag{69}$$

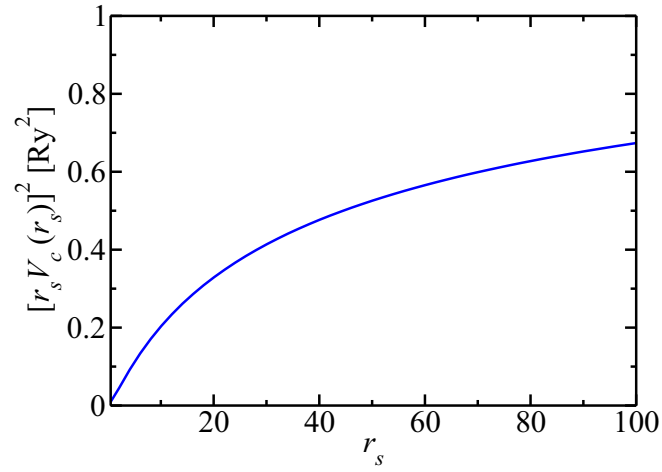

FIG. 1. Plot of the square of $V_c r_s$ vs r_s. r_s is the dimensionless density parameter defined in Eq. (68).

and

$$M^{(3+)}_{\sigma nm} = \int d^3r \mathcal{V}^{(3+)}_{\sigma}(\boldsymbol{r})\phi^*_n(\boldsymbol{r})\phi_m(\boldsymbol{r}). \tag{70}$$

While it might be tempting to use these expansions, Eqs. (66) and (67), to compute the moment functionals it is instructive to recall first the parametrization of the correlation energy of the uniform electron gas.

In order to construct an accurate analytic representation of the correlation energy of the uniform electron gas, one considers the high-density expansion, the low-density expansion, and Green's function Monte Carlo data [25]. In the low-density expansion, the leading order is r_s^{-1} for the exact correlation energy. In the high-density limit, one considers instead the parametrization $c_0(\zeta)\ln r_s - c_1(\zeta) + c_2(\zeta)r_s\ln r_s$. Since these two functional forms for the low- and high-density limits differ considerably, we cannot expect good results, if we construct moment functionals only based on the parameterizations Eqs. (66) and (67), which describe the case of low density. To give an impression of the deviation of the correlation energy density ϵ_c from the low-density behavior $\propto r_s^{-1}$, we plot in Fig. 1 the quantity $[V_c r_s]^2$, where

$$V_c = \frac{d(\epsilon_c n)}{dn}. \tag{71}$$

In order to take into account Monte Carlo simulations in the construction of the moment functionals, we would need such calculations for correlation functions such as Eq. (19) through Eq. (35) for the uniform electron gas. Since these data are currently not available in the literature, we nevertheless use the parametrization Eq. (66) in our applications below. As in this paper we present our first tests of the MFbSDFT-method, this slightly crude approach is justified, because the development of accurate moment functionals will probably take similarly long as the development of the modern functionals used in KS-DFT calculations. Therefore it is important to demonstrate the feasibility of the method before developing accurate moment functionals.

Additionally, we test the following strategy to find more elaborated moment functionals: Eq. (66) suggests that the

leading order at low density is r_s^{-2}. Since the leading order of the correlation energy is r_s^{-1} in this limit, we try to replace r_s^{-2} in Eq. (66) by the square of the correlation potential V_c, i.e.,

$$\mathcal{V}_\sigma^{(2+)}(\boldsymbol{r}) = d_\sigma^{(2+)}[V_c(r_s)]^2 \tag{72}$$

and similarly

$$\mathcal{V}_\sigma^{(3+)}(\boldsymbol{r}) = d_\sigma^{(3+)}[V_c(r_s)]^3. \tag{73}$$

This strategy should yield better results, because the r_s^{-2} and r_s^{-3} of the low-density expansion are hereby replaced by a more realistic functional form at high density.

In Appendix B, we have estimated Eq. (19) through Eq. (35) based on zeroth-order perturbation theory. According to this estimate, the prefactor of r_s^{-2} is of the order of 10[Ry]^2. The prefactor of r_s^{-1} in the low-density expansion of the correlation potential is of the order of 1.2[Ry]. When we use the square of the correlation energy we have to choose the prefactor $d_\sigma^{(2+)}$ of the square of the correlation energy so that $d_\sigma^{(2+)}(1.2r_s^{-1})^2$ becomes comparable to $10r_s^{-2}$. We therefore expect $d_\sigma^{(2+)}$ to be of the order of 10. At this order of magnitude of $d_\sigma^{(2+)}$ we indeed find a strong satellite peak in Ni (see Sec. VI).

V. SECOND VARIATION APPROACH

In this section, we describe the implementation of our MFbSDFT method within a second variation approach. By second variation we mean that first a standard KS Hamiltonian is diagonalized at a given k point and only part of its eigenvectors are used to compute the matrix elements of the moment functionals. The computation of the state vector matrix $\boldsymbol{\mathcal{V}}$ and of the energies $E_l = \mathcal{D}_{ll}$ may therefore be considered as a second variation step.

The size of the KS Hamiltonian matrix depends on the number of basis functions N_B. We do not compute all eigenvectors, but only as many eigenvectors as we need to describe the occupied bands and a fraction of the unoccupied bands. We call this number $N < N_\mathrm{B}$. At a given k point, we additionally compute the $N_\mathrm{B}\times N_\mathrm{B}$ matrices $\boldsymbol{M}^{(2+)}$ and $\boldsymbol{M}^{(3+)}$ and project them onto the N eigenstates. By $\bar{\boldsymbol{M}}^{(2+)}$ and $\bar{\boldsymbol{M}}^{(3+)}$ we denote these projections:

$$\bar{\boldsymbol{M}}^{(2+)} = \bar{\boldsymbol{U}}^\dagger \boldsymbol{M}^{(2+)} \bar{\boldsymbol{U}} \tag{74}$$

and

$$\bar{\boldsymbol{M}}^{(3+)} = \bar{\boldsymbol{U}}^\dagger \boldsymbol{M}^{(3+)} \bar{\boldsymbol{U}}, \tag{75}$$

where $\bar{\boldsymbol{U}}$ is a $N_\mathrm{B}\times N$ matrix, which holds the N eigenvectors in its N columns.

The implementation of the moments $\boldsymbol{M}^{(2+)}$ and $\boldsymbol{M}^{(3+)}$ is easy to do. In the subroutines computing the standard KS-Hamiltonian one needs to switch off the kinetic energy contribution such that only the computation of the matrix elements of the potential remains. If one additionally replaces the exchange-correlation potential by the moment functional potential for $\boldsymbol{M}^{(2+)}$ or $\boldsymbol{M}^{(3+)}$, the subroutine computes the corresponding moment matrix.

The first and zeroth moments in the basis of the N eigenstates are diagonal matrices:

$$\bar{M}_{nm}^{(1)} = E_n^\mathrm{HF}\delta_{nm} \tag{76}$$

and

$$\bar{M}_{nm}^{(0)} = \delta_{nm}. \tag{77}$$

Note that in contrast to a standard KS-DFT calculation, the KS-Hamiltonian used in the first variation step does not use the full exchange-correlation potential, but only the local or nonlocal first-order exchange, i.e., either Eq. (11) or Eq. (13). Therefore we denote the band energies from the first variation step by E_n^HF in Eq. (76). Moments and band energies depend additionally on the k point if periodic boundary conditions are used, but we suppress again the k index in the moments and also in the band energy, i.e., instead of $E_{\boldsymbol{k}n}^\mathrm{HF}$ we write E_n^HF.

The second and third moments are given by

$$\bar{\boldsymbol{M}}^{(2)} = \bar{\boldsymbol{M}}^{(1)}\bar{\boldsymbol{M}}^{(1)} + \bar{\boldsymbol{M}}^{(2+)} \tag{78}$$

and

$$\bar{\boldsymbol{M}}^{(3)} = \bar{\boldsymbol{M}}^{(1)}\bar{\boldsymbol{M}}^{(1)}\bar{\boldsymbol{M}}^{(1)} + \bar{\boldsymbol{M}}^{(3+)}, \tag{79}$$

respectively.

The size of the matrices $\bar{\boldsymbol{M}}^{(0)}$, $\bar{\boldsymbol{M}}^{(1)}$, $\bar{\boldsymbol{M}}^{(2)}$, and $\bar{\boldsymbol{M}}^{(3)}$ is $N\times N$ and typically $N \ll N_\mathrm{B}$. Therefore the second variation approach is fast.

Close to the end of the self-consistency cycle the Fermi energy is determined such that the total electronic charge compensates the nuclear charge. Typically, the subroutine computing the Fermi energy makes use of the eigenvalues and of weights, which are determined by the multiplicities of the k points, when symmetries are used. In order to include the spectral weights Eq. (63) into the calculation of the Fermi energy, one only needs to multiply the k-point weights with these spectral weights. Similarly, the spectral weights need to be considered when computing the charge density from the matrix $\boldsymbol{\mathcal{V}}$ of state vectors, Eq. (64), according to

$$n(\boldsymbol{r}) = \sum_{\sigma nmj} \phi_n^*(\boldsymbol{r})\phi_m(\boldsymbol{r}) a_{j\sigma} \mathcal{V}_{nj\sigma}^* \mathcal{V}_{mj\sigma} f(E_{j\sigma}), \tag{80}$$

which may be derived from Eq. (14) by using the spectral theorem [17] to express the correlator $\langle c_{\sigma n}^\dagger c_{\sigma m}\rangle$ in terms of the spectral function.

We illustrate the self-consistency loop by the flowchart in Fig. 2. All results presented in Sec. VI have been obtained according to the flowchart in Fig. 2.

KS-DFT is so constructed that it may be used to obtain the total energy and the charge density in principle exactly. However, in practice the exact exchange correlation potential is not known and therefore the charge density computed in KS-DFT is an approximation. Since considerable progress has been made in the construction of exchange correlation potentials, the KS charge density is a very good approximation in many cases. Whenever the KS charge density is sufficiently correct, one may run MFbSDFT in a simplified mode: The converged KS charge density is used as starting density in Fig. 2 and only one iteration is performed, i.e., the output charge density is not computed but instead the results are

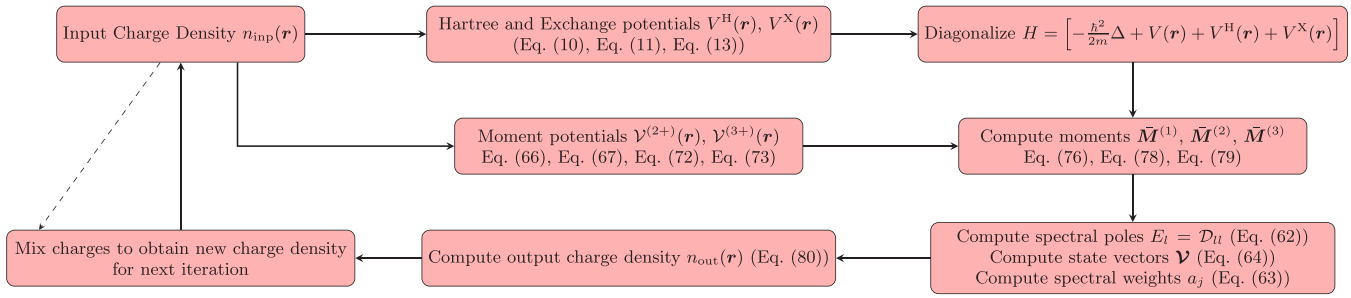

FIG. 2. Flowchart of the MFbSDFT self-consistency cycle.

calculated immediately from the state vector matrix $\boldsymbol{\mathcal{V}}$, from the spectral poles, and from the spectral weights.

VI. APPLICATIONS

In this section, we apply the MFbSDFT method to several well-studied materials that show genuine many-body effects such as satellite peaks. According to the literature, the details of the spectral function of these materials depend strongly on the theoretical model used to study them. According to our discussion in Sec. IV, the parametrizations that we use for the moment functionals should be considered only as a first step towards the development of accurate moment functionals. Consequently, if the results shown below are more similar to one theoretical model than they are to another one this does not imply at all that MFbSDFT confirms one particular theoretical model, because accurate moment functionals remain to be developed. The main purpose of this section is therefore to show that MFbSDFT is able to reproduce spectral features qualitatively that have been identified as genuine correlation effects before.

However, beyond validating the concept of MFbSDFT, the results shown also hint at a practical perspective for MFbSDFT already at this early stage of its development. Since the MFbSDFT reproduces spectral features of correlated materials, it may be used to compute response properties [17] such as the anomalous Hall effect, which is likely to require considerably less computer time than LDA+DMFT. For such an application one would fine-tune the parameters in the parameterizations of the moment functionals to match the spectral function known from LDA+DMFT or photoemission. While this approach is not parameter-free, it is similar to many applications of LDA+U, where the U parameter is chosen to reproduce a material property.

A. Fcc Ni

The DOS obtained in KS-DFT with the PBE functional is shown in Fig. 3. The valence DOS starts to become significant starting from 5 eV below the Fermi energy and the exchange splitting is around 0.75 eV. In contrast, the width of the main bands found experimentally is significantly smaller than 5 eV, namely, only 3 eV. Additionally, a much smaller exchange splitting of around 0.3 eV is found in photoemission experiments [30,31]. Moreover, the satellite peak observed in experiments at around 6 eV below the Fermi energy is absent in the KS-DFT spectrum.

Next, we discuss the MFbSDFT-spectrum obtained with $\mathcal{V}_\sigma^{(2+)}(\boldsymbol{r}) = 15\zeta_\sigma^{(5/3)}[V_c(r_s)]^2$ and $\mathcal{V}_\sigma^{(3+)}(\boldsymbol{r}) = 0$. Here $\zeta_\sigma = (1 - \sigma(n_\uparrow - n_\downarrow)/n)$. We use $N = 36$. With this choice of parameters the magnetic moment computed self-consistently in MFbSDFT is $0.58\,\mu_{\mathrm{B}}$. The resulting DOS is presented in Fig. 4. The exchange splitting of around 0.3 eV is strongly reduced compared to the KS-DFT calculation and close to the experiments [30,31]. Additionally, the main bands are much narrower than in KS-DFT and therefore in much better agreement with experiments. Moreover, satellite peaks are found close to 6 eV. However, the spectral weight of these satellite peaks is smaller than what is found in experiments and in LDA+DMFT calculations (see, e.g., Fig. 9 in Ref. [32], Fig. 2 in Ref. [14], and Fig. 2 in Ref. [33]).

Finally, we discuss the MFbSDFT-spectrum obtained with $\mathcal{V}_\sigma^{(2+)}(\boldsymbol{r}) = 0.015\zeta_\sigma^{(7/3)} r_s^{-2}$ [Ry]^2 and $\mathcal{V}_\sigma^{(3+)}(\boldsymbol{r}) = -0.00472\zeta_{-\sigma}^{(1/3)} r_s^{-3}$ [Ry]^3. We use $N = 36$. With this choice of parameters the magnetic moment is $0.63\,\mu_{\mathrm{B}}$. Figure 5 shows the density of states (DOS) of Ni in the ferromagnetic state as computed selfconsistently in MFbSDFT. While the exchange splitting is similar to KS-DFT, the width of the main bands is reduced, leading to a slightly better agreement with experiment. Around 6 eV below the Fermi energy satellite peaks appear with a spectral weight of a similar order of magnitude like in experiment and LDA+DMFT. However,

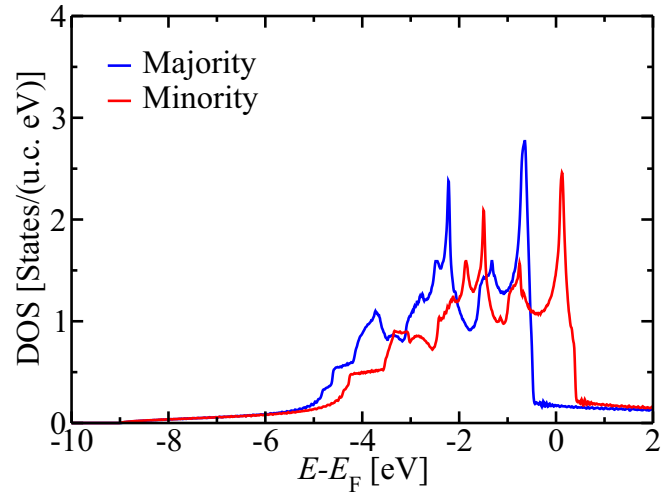

FIG. 3. DOS of Ni vs energy E in the ferromagnetic state as obtained in KS-DFT. E_{F} is the Fermi energy.

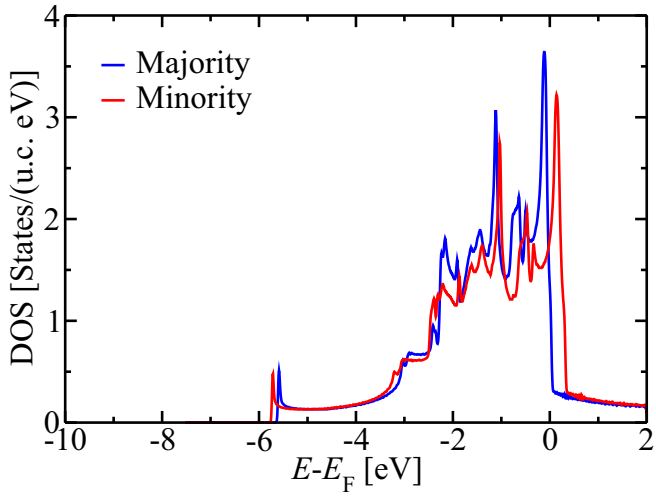

FIG. 4. DOS of Ni vs energy E in the ferromagnetic state as obtained in MFbSDFT when the moment functional is constructed according to Eq. (72). E_F is the Fermi energy.

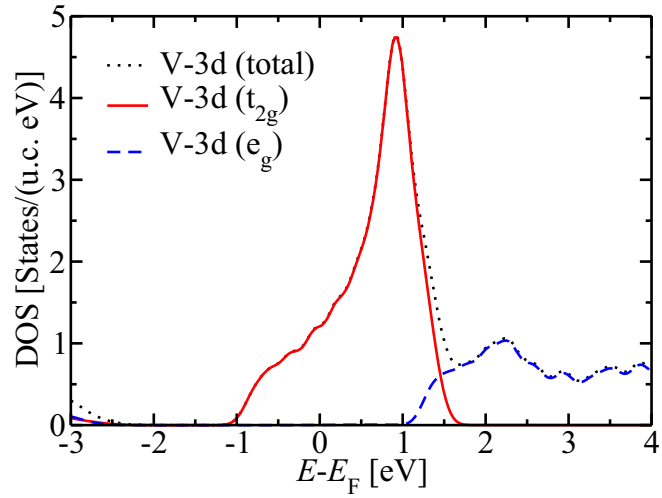

FIG. 6. Contributions of the V-3d e_g and t_{2g} states to the DOS in $SrVO_3$. Results from KS-DFT using the PBE functional.

the spin polarization of the satellite peak structure differs from both experiment and LDA+DMFT, which both predict the minority satellite to be strongly suppressed (see e.g. Fig. 9 in Ref. [32], Fig. 2 in Ref. [14], and Fig. 2 in Ref. [33]). In contrast, in Fig. 5, the satellites of the majority and minority band are comparable in magnitude and only shifted in energy.

As discussed in Sec. IV the parameters employed in $\mathcal{V}_\sigma^{(2+)}(\boldsymbol{r}) = 15\zeta_\sigma^{(5/3)}[V_c(r_s)]^2$ (used to generate the DOS shown in Fig. 4) are of the order of magnitude expected from the estimate given in Sec. IV. In contrast, we determined the parameters employed in $\mathcal{V}_\sigma^{(2+)}(\boldsymbol{r}) = 0.015\zeta_\sigma^{(7/3)}r_s^{-2}$ [Ry]^2 (used to generate the DOS shown in Fig. 5) only based on try-out, because it is unclear how to renormalize the parameters of the low-density expansion so that it effectively describes the regimes of intermediate and high densities as well. However, Fig. 5 is useful nevertheless, because it shows that satellite peaks with the correct order of magnitude of spectral weight can be produced by MFbSDFT. Taken together with the result of Fig. 4, which shows that band widths, exchange splittings and location of the satellite peaks are predicted very well if the correlation potential is used to construct the moment functionals, the overall conclusion from this finding is that it is likely that assessing Eq. (19) through Eq. (35) in the low-density and the high-density regimes and using Monte Carlo results to interpolate between these limits will allow us to formulate a moment functional that predicts the spectral features in Ni quite well.

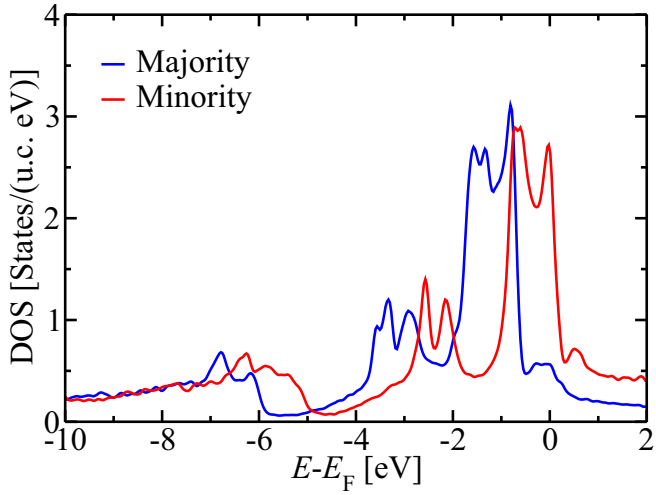

FIG. 5. DOS of Ni vs energy E in the ferromagnetic state as obtained in MFbSDFT when the moment functional is constructed according to Eqs. (66) and (67). E_F is the Fermi energy.

B. $SrVO_3$

In Fig. 6, we show the contributions of the V-3d e_g and t_{2g} states to the DOS of $SrVO_3$, as obtained with KS-DFT using the PBE functional. The KS spectrum is not in good agreement with experiment. It has been shown that the agreement with experiment is improved significantly [11], when DMFT is used to supplement these bands with correlation effects. The detailed rearrangement of the spectral features obtained from LDA+DMFT depends on the details of the modeling of the correlation effects by the Hubbard model. Ref. [11] includes only the t_{2g} states into the Hubbard model. In this case the DOS of the t_{2g} states obtained from LDA+DMFT is distributed into three pronounced spectral peaks: A dominant central peak roughly 0.5 eV above the Fermi energy, a lower Hubbard band around 2 eV below the Fermi energy and an additional upper Hubbard band around 3 eV above the Fermi energy. The position of these peaks is in good agreement with experiments, which find peaks roughly at -1.7, 0.5, and 2.4 eV [34,35]. These spectral features are also observed in Ref. [36], which includes the e_g states, however they strongly depend on the parameters, and the intensities of the lower and upper Hubbard bands are much smaller for some parameters. Additionally, the intensities of the lower and upper Hubbard bands depend strongly on the double counting correction.

In Fig. 7, we present the contributions of the V-3d e_g and t_{2g} states to the DOS, as obtained with MFbSDFT when

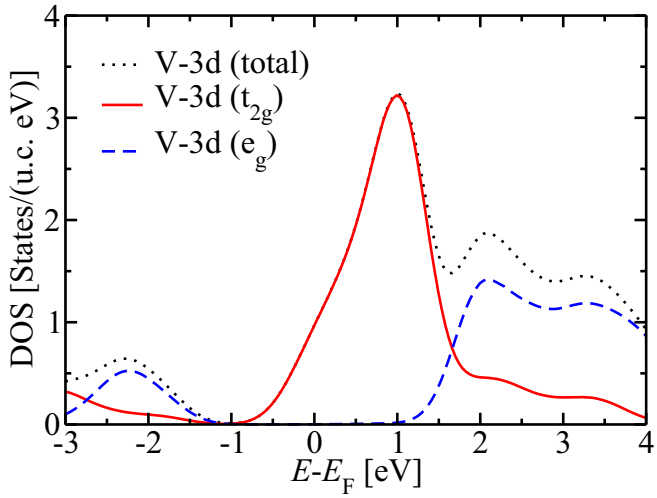

FIG. 7. Contributions of the V-3d e_g and t_{2g} states to the DOS in $SrVO_3$. Results obtained within MFbSDFT when the moment functionals are constructed according to Eqs. (72) and (73).

we use Eqs. (72) and (73), where we set $d_\sigma^{(2+)} = 100$ and $d_\sigma^{(3+)} = -200$. We use $N = 200$. The total V-d DOS is in good agreement with both the experimental spectrum and the LDA+DMFT spectrum (see, e.g., Fig. 7 in Ref. [11] for comparison. Reference [11] uses a broadening of 0.36 eV in order to reproduce the experimental resolution. We use 0.36 eV in our Fig. 7 as well.). However, in our case the peak between 2 eV and 2.5 eV stems mainly from the e_g states, which are not included into the Hubbard model in Ref. [11]. Reference [36] includes the e_g states, but still finds a small peak from the upper Hubbard band for the t_{2g} states at around 3 eV above the Fermi energy. Such a small peak is consistent with our Fig. 7, where a shoulder in the V-3d(t_{2g}) is clearly visible between 2 eV and 2.5 eV. Moreover, Ref. [36] finds a large contribution from the e_g states to the DOS at this energy as well. In this regard, our Fig. 7 resembles closely Fig. 8 in Ref. [36] when

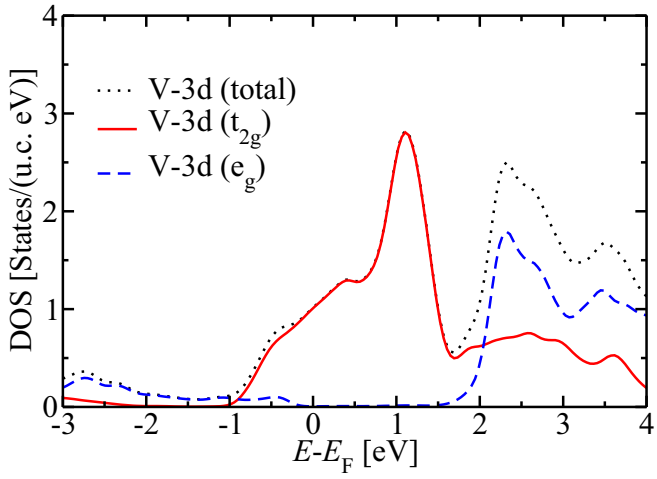

FIG. 8. Contributions of the V-3d e_g and t_{2g} states to the DOS in $SrVO_3$. Results obtained within MFbSDFT when the moment functionals are constructed according to Eqs. (66) and (67).

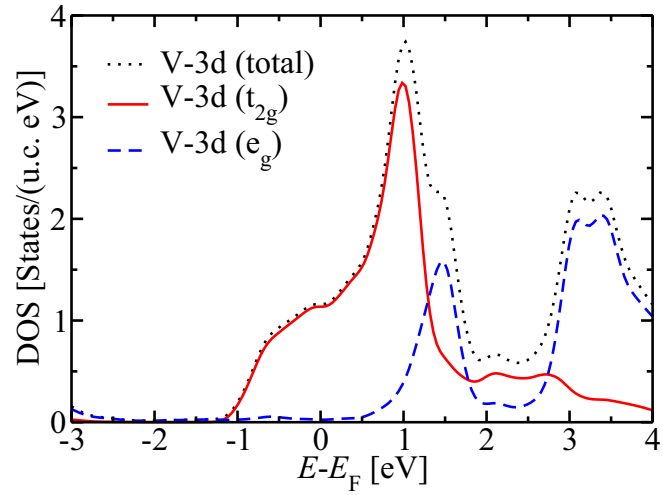

FIG. 9. Contributions of the V-3d e_g and t_{2g} states to the DOS in $SrVO_3$. Results obtained within MFbSDFT when the moment functionals are constructed according to Eqs. (66) and (67). In contrast to Fig. 8 the parameters $c_\sigma^{(2+)}$ and $c_\sigma^{(3+)}$ are reduced by 18% and 33%, respectively.

the energy is above the Fermi energy. However, Fig. 8 in Ref. [36] does not find a strong V-d DOS at around 2 eV below the Fermi energy. In contrast, we find a strong V-d DOS at around 2 eV below the Fermi energy with a dominant part from the e_g states and a small contribution from the t_{2g} states.

In Fig. 8, we show the contributions of the V-3d e_g and t_{2g} states to the DOS, as obtained with MFbSDFT when we take $N = 200$ and use Eqs. (66) and (67), where we set $c_\sigma^{(2+)} = 1.1$ [Ry]^2, and $c_\sigma^{(3+)} = -1.5$ [Ry]^3. The peak between 2 and 2.5 eV is very pronounced and both e_g and t_{2g} bands contribute to it. In contrast, the peak around -2 eV in Fig. 7 is significantly smaller in Fig. 8 and shifted to lower energy between -2.5 eV and -3 eV. Several main features of the t_{2g} band in Fig. 8 resemble those obtained from a LDA+DMFT calculation with a Hubbard U of 6 eV (see Fig. 8 in Ref. [36]). Notably, the t_{2g} band, which ends around 2 eV in Fig. 6, is expanded to higher energies like in LDA+DMFT. Overall, the total V-d DOS in Fig. 8 is qualitatively similar to the one in Fig. 8 of Ref. [36], which displays pronounced peaks close to 1 eV and close to 2.5 eV, while the V-d DOS close to -2 eV is small, in agreement with our result in Fig. 8. However, the peak close to 2.5 eV is much larger in our Fig. 8.

We may reduce the intensity of this peak at 2.5 eV by reducing the parameters $c_\sigma^{(2+)}$ and $c_\sigma^{(3+)}$. In Fig. 9, we show the DOS obtained with the parameters $c_\sigma^{(2+)} = 0.9$[Ry]^2 and $c_\sigma^{(3+)} = -1$[Ry]^3. Indeed, the peak intensity is reduced and it is now significantly smaller than the intensity of the main peak at around 1 eV, but relative to the main peak it is still more pronounced than in Fig. 8 of Ref. [36]. Moreover, the peak is shifted from 2.5 eV in our Fig. 8 to higher energies and lies now between 3 eV and 3.5 eV. However, overall the total V-d DOS, the V-3d (t_{2g}) DOS, and the V-3d (e_g) DOS in Fig. 8 of Ref. [36] is in better agreement with our Fig. 9 than with our Fig. 8.

VII. DISCUSSION AND OUTLOOK

In the previous section, we have shown that MFbSDFT reproduces features such as satellite peaks and spectral weight shifts which are usually obtained by solving the correlated electron problem directly, e.g., by means of LDA+DMFT. While these first MFbSDFT results look therefore very promising there is a large number of open questions and obvious possibilities to improve this method further.

First, accurate moment functionals are required. The construction of accurate moment functionals should be possible based on Monte Carlo data of correlation functions such as those given in Eq. (19) through Eq. (35).

Second, it is desirable to derive gradient approximations for the moment functionals. Using local functionals that depend only on the spin densities for MFbSDFT misses effects related to their spatial inhomogeneity. Like GGA is an improvement over LDA, we expect that MFbSDFT will become more accurate by adding gradient corrections to the functionals.

Third, in this work, we do not explore the calculation of total energies and atomic forces for structural relaxation. However, since force calculations in correlated materials are possible within LDA+DMFT we expect that total energies and forces may also be obtained within our MFbSDFT approach.

Fourth, one may use more than the first four moments. While the first four moments are sufficient to reproduce the quasi-particle band structure qualitatively correctly in the strong-correlation regime [37], the precision of MFbSDFT is expected to increase with the number of moments used. The moments become increasingly more complicated with increasing order. However, one may use computer algebra systems in order to derive the higher-order moments and to assess them for the uniform electron gas. This seems feasible since the complexity is probably comparable to higher-order perturbation theory in QED, where high-order contributions have to be tackled by computer algebra. Assuming that computer algebra systems can manage the complexity of the higher-order moments the question remains if the spectral function can be found for more than 2 or 4 moments. In Ref. [17], we give an argument that the spectral function may be found from the first four moments, which is based on counting the number of available equations and the number of parameters that determine the spectral function and showing that these numbers match. In the present paper, we have explicitly constructed the spectral function from the first four moments in Sec. III. We may generalize the argument given in Ref. [17] and show that from the first $2P$ moments ($P = 1, 2, \dots$) one may construct the spectral function. This generalization is discussed in Appendix E. If one uses only Delta functions in the expression for the spectral function [as in Eq. (65)] one misses lifetime effects, which may be accommodated by employing Gaussians instead [38]. When four moments are required to put the spectral peaks, such as satellite peaks, at the right energies, it is clear that more than four moments are generally required to correct the spectral widths of these spectral features by lifetime effects.

Fifth, perhaps the method of spectral moments may contribute to the understanding of SIE, because it is remarkable that setting $\mu_c(\boldsymbol{r}) = 0$ in Eq. (2.22) of Ref. [2] leads to a HF-type method that suffers from the same SIE and is equivalent to the method of spectral moments derived from the first two moments (see Sec. II). We suspect that increasing the number of moments used will ultimately eliminate the SIE. However, it is an open question, how the self-interaction correction (SIC) takes place exactly within the method of spectral moments. Within the KS-DFT framework the explanation of SIC is that $\mu_c(\boldsymbol{r})$ in Eq. (2.22) of Ref. [2] has to eliminate SIE when the exact exchange correlation functional is used. However, within the spectral moment method a valid explanation of SIE seems to be that using only the first two moments produces an error, which may be eliminated by using more moments. Of course, the precise moment functionals are expected to be necessary in order to remove SIE. However, Eq. (19) through Eq. (35) provide explicit expressions, which may be used for the construction of the moment functionals.

Sixth, it is an important open question how to extend the MFbSDFT approach to finite temperatures. In Ref. [17], we have shown how to generalize the spectral moment method so that it can be applied to many-band Hamiltonians. Since the method of Ref. [17] computes the correlation functions from the spectral theorem, which involves the Fermi function and the actual excitation energies, it naturally includes finite temperature effects. As the spectral theorem is not used for the higher-order correlation functions in MFbSDFT, which are obtained from moment functionals, it is currently unknown how to accomodate finite temperatures accurately in this method.

While accurate moment functionals are currently not available yet, the MFbSDFT method may also be used in practice in a way similar to LDA+U. In LDA+U, the U and J parameters are usually chosen for a given material in order to add correlation effects that are not described by LDA. Similarly, one may use parametrizations of the moment functionals similar to the ones that we discussed in Sec. IV and choose the coefficients in the functional in order to optimize spectral features.

VIII. SUMMARY

We describe the concept of moment functionals, which allow us to obtain the spectral moments from functionals of the charge density. These functionals play a similar role in MFbSDFT as the exchange correlation functional does in KS-DFT. We derive explicit expressions for the moment functionals and use perturbation theory to investigate their scaling with the charge density. We describe an efficient algorithm to obtain the spectral function from the first four spectral moments. We demonstrate that MFbSDFT allows us to reproduce spectral features such as satellite peaks in Ni and lower and upper Hubbard bands in $SrVO_3$. At this stage of its development, MFbSDFT may be used in a way similar to LDA+U: The parameters in the moment functionals are chosen such that spectral features found in experiments are reproduced.

ACKNOWLEDGMENTS

The project is funded by the Deutsche Forschungsgemeinschaft (DFG, German Research Foundation)–TRR

288–422213477 (Project No. B06), CRC 1238, Control and Dynamics of Quantum Materials: Spin orbit coupling, correlations, and topology (Project No. C01), SPP 2137 "Skyrmionics", and Sino-German research project DISTOMAT (DFG Project No. MO 1731/10-1). We also acknowledge financial support from the European Research Council (ERC) under the European Union's Horizon 2020 research and innovation program (Grant No. 856538, project "3D MAGiC") and computing resources granted by the Jülich Supercomputing Centre under Project No. jiff40.

APPENDIX A: COMPARISON OF THE SPECTRAL MOMENTS OF THE MANY-BAND CASE TO THE SPECTRAL MOMENTS OF THE SINGLE-BAND HUBBARD MODEL

The spectral moments of the many-band case contain many new contributions that do not have counterparts in the single-band Hubbard model. In this Appendix, we discuss which of the many-band terms have a correspondence in the single-band Hubbard model. In the single band Hubbard model, the Coulomb matrix element is simply

$$V_{nn'tt'} = U\delta_{nn'}\delta_{tt'}\delta_{nt}, \tag{A1}$$

where U is the Hubbard U. For the single band Hubbard model the first four moments are

$$\tilde{M}^{(0)}_{\boldsymbol{k}\sigma} = \frac{1}{\mathcal{N}}\sum_{lj} e^{i\boldsymbol{k}\cdot(\boldsymbol{R}_l-\boldsymbol{R}_j)}\langle[c_{\sigma l}, c^\dagger_{\sigma j}]_+\rangle = 1, \tag{A2}$$

$$\begin{aligned}\tilde{M}^{(1)}_{\boldsymbol{k}\sigma} &= \frac{1}{\mathcal{N}}\sum_{lj} e^{i\boldsymbol{k}\cdot(\boldsymbol{R}_l-\boldsymbol{R}_j)}\langle[[c_{\sigma l}, H]_-, c^\dagger_{\sigma j}]_+\rangle \\ &= \epsilon(\boldsymbol{k}) + U\langle n_{-\sigma}\rangle,\end{aligned} \tag{A3}$$

$$\begin{aligned}\tilde{M}^{(2)}_{\boldsymbol{k}\sigma} &= \frac{1}{\mathcal{N}}\sum_{lj} e^{i\boldsymbol{k}\cdot(\boldsymbol{R}_l-\boldsymbol{R}_j)}\langle[[[c_{\sigma l}, H]_-, [H, c^\dagger_{\sigma j}]_-]_+\rangle \\ &= (\epsilon(\boldsymbol{k}))^2 + 2U\langle n_{-\sigma}\rangle\epsilon(\boldsymbol{k}) + U^2\langle n_{-\sigma}\rangle,\end{aligned} \tag{A4}$$

and

$$\begin{aligned}\tilde{M}^{(3)}_{\boldsymbol{k}\sigma} &= \frac{1}{\mathcal{N}}\sum_{lj} e^{i\boldsymbol{k}\cdot(\boldsymbol{R}_l-\boldsymbol{R}_j)}\langle[[[[c_{ls}, H]_-, H]_-, H], c^\dagger_{js}]_-]_+\rangle \\ &= [\epsilon(\boldsymbol{k})]^3 + 3U\langle n_{-\sigma}\rangle[\epsilon(\boldsymbol{k})]^2 \\ &\quad + 2U^2\epsilon(\boldsymbol{k})n_{-\sigma} + 2U^2 t_{00}n_{-\sigma} + U^3 n_{-\sigma} \\ &\quad - U^2\frac{1}{\mathcal{N}}\sum_{lj} e^{i\boldsymbol{k}\cdot(\boldsymbol{R}_l-\boldsymbol{R}_j)}t_{lj}\langle c^\dagger_{-\sigma l}c^\dagger_{-\sigma j}c_{-\sigma l}c_{-\sigma j}\rangle \\ &\quad + U^2\frac{1}{\mathcal{N}}\sum_{lj} t_{lj}\langle(2n_{\sigma l}-1)c^\dagger_{-\sigma l}c_{-\sigma j}\rangle \\ &\quad + U^2\frac{1}{\mathcal{N}}\sum_{lj} e^{i\boldsymbol{k}\cdot(\boldsymbol{R}_l-\boldsymbol{R}_j)}t_{lj}\langle c^\dagger_{\sigma j}c^\dagger_{-\sigma l}c_{\sigma l}c_{-\sigma j}\rangle \\ &\quad + U^2\frac{1}{\mathcal{N}}\sum_{lj} e^{i\boldsymbol{k}\cdot(\boldsymbol{R}_l-\boldsymbol{R}_j)}t_{lj}\langle c^\dagger_{\sigma j}c^\dagger_{-\sigma j}c_{\sigma l}c_{-\sigma l}\rangle.\end{aligned} \tag{A5}$$

Here, $\mathcal{N}$ is the number of $\boldsymbol{k}$ points.

Clearly, Eqs. (8) and (9) turn into Eqs. (A2) and (A3), respectively, when one evaluates them for the single-band Hubbard model and performs a Fourier transformation.

The following contributions to $M^{(2+)}$ are zero for the single-band Hubbard model: $M^{(2+,3)}$, $M^{(2+,4)}$, $M^{(2+,5)}$, $M^{(2+,6)}$, and $M^{(2+,7)}$. The sum $M^{(2+,1)} + M^{(2+,2)}$ turns into $U^2\langle n_{-\sigma}\rangle$ in the single-band case, which is the last term in Eq. (A4). The sum $\boldsymbol{T}\boldsymbol{V}^{\mathrm{H}} + \boldsymbol{T}\boldsymbol{V}^{\mathrm{X}}_\sigma + \boldsymbol{V}^{\mathrm{H}}\boldsymbol{T} + \boldsymbol{V}^{\mathrm{X}}_\sigma\boldsymbol{T}$, which contributes to Eq. (16), evaluates to $2U\langle n_{-\sigma}\rangle\epsilon(\boldsymbol{k})$ in the case of the single-band Hubbard model. This is the middle term in Eq. (A4).

For the single-band Hubbard model the sum of $M^{(3+,3)}_{nm}$ [Eq. (50)] and $M^{(3+,4)}_{\sigma nm}$ [Eq. (51)] is $U^3\langle n_{-\sigma}\rangle$, which is the last term in the third line of Eq. (A5).

APPENDIX B: EVALUATION OF $M^{(2+,j)}_{\sigma nm}$

In order to keep the notation simple, we discuss the contractions $\mathcal{C}^{(2+,j)}_\sigma$, Eq. (36), for the uniform electron gas without spin polarization.

We evaluate the contraction of Eq. (20) by transforming it into the momentum representation, where we obtain at zero temperature

$$\begin{aligned}\mathcal{C}^{(2+,2)}_\sigma &= -\int \frac{d^3q d^3k_4 d^3k_5}{(2\pi)^9 n V^{-2}} v(\boldsymbol{q})v(\boldsymbol{k}_4-\boldsymbol{k}_5+\boldsymbol{q})n_{\boldsymbol{k}_5-\boldsymbol{q}}n_{\boldsymbol{k}_4+\boldsymbol{q}} \\ &= -A_2\int d^3q d^3k_4 d^3k_5 \\ &\quad\times \frac{\Theta(k_{\mathrm{F}}-|\boldsymbol{k}_5-\boldsymbol{q}|)\Theta(k_{\mathrm{F}}-|\boldsymbol{k}_4+\boldsymbol{q}|)}{q^2|\boldsymbol{k}_4-\boldsymbol{k}_5+\boldsymbol{q}|^2}.\end{aligned} \tag{B1}$$

Here,

$$k_{\mathrm{F}} = (3\pi^2 n)^{1/3} \tag{B2}$$

is the Fermi wave number, $\Theta(k)$ is the Heaviside step function,

$$v(\boldsymbol{q}) = \frac{8\pi}{V}[\mathrm{Ry}][a_{\mathrm{B}}]\frac{1}{q^2} \tag{B3}$$

is the Coulomb potential expressed in terms of the Bohr radius a_{B}, Ry = 13.6 eV, and

$$A_2 = \frac{(8\pi)^2}{(2\pi)^9}[\mathrm{Ry}]^2[a_{\mathrm{B}}]^2\frac{1}{n}. \tag{B4}$$

Scaling all momenta in Eq. (B1) by the factor ξ, we observe that this integral is proportional to ξ^2, i.e., it is proportional to k_{F}^2. In this scaling analysis we took into account that n depends on k_{F} as well: $n = k_{\mathrm{F}}^3/(3\pi^2)$. It is convenient to express $\mathcal{C}^{(2+,2)}_\sigma$ in terms of the dimensionless density parameter

$$r_s = \frac{1}{a_{\mathrm{B}}}\left(\frac{9\pi}{4k_{\mathrm{F}}^3}\right)^{\frac{1}{3}}. \tag{B5}$$

According to the scaling analysis above, it is sufficient to evaluate the integral for a single density parameter, e.g., $r_s' = 1$, because

$$\mathcal{C}^{(2+,2)}_\sigma(r_s) = \frac{\mathcal{C}^{(2+,2)}_\sigma(r_s'=1)}{r_s^2}. \tag{B6}$$

The integral can be performed numerically using the VEGAS [39,40] package for the Monte Carlo integration of high-dimensional integrals. We obtain

$$\mathcal{C}^{(2+,2)}(r_s) = \frac{-2.57}{r_s^2}[\mathrm{Ry}]^2. \tag{B7}$$

Next, we consider $\mathcal{C}^{(2+,16)}$. This integral is given by

$$\begin{aligned}\mathcal{C}_\sigma^{(2+,16)} &= \int \frac{d^3q d^3k_4 d^3k_5}{(2\pi)^9 n V^{-2}} v(\boldsymbol{q}) \\ &\quad \times v(\boldsymbol{k}_4 - \boldsymbol{k}_5 + \boldsymbol{q}) n_{\boldsymbol{k}_5-\boldsymbol{q}} n_{\boldsymbol{k}_4+\boldsymbol{q}} n_{\boldsymbol{k}_5} \\ &= A_2 \int d^3q d^3k_4 d^3k_5 \Theta(k_\mathrm{F} - |\boldsymbol{k}_5|) \\ &\quad \times \frac{\Theta(k_\mathrm{F} - |\boldsymbol{k}_5 - \boldsymbol{q}|)\Theta(k_\mathrm{F} - |\boldsymbol{k}_4 + \boldsymbol{q}|)}{q^2 |\boldsymbol{k}_4 - \boldsymbol{k}_5 + \boldsymbol{q}|^2},\end{aligned} \tag{B8}$$

which also scales like r_s^{-2}, which is easy to see with a scaling analysis. Evaluating this integral with the VEGAS [39,40] package gives

$$\mathcal{C}^{(2+,16)}(r_s) = \frac{1.73}{r_s^2}[\mathrm{Ry}]^2. \tag{B9}$$

For the contraction $\mathcal{C}^{(2+,17)}$, we need to compute the integral

$$\begin{aligned}\mathcal{C}_\sigma^{(2+,17)} &= \int \frac{d^3q d^3k_4 d^3k_5}{(2\pi)^9 n V^{-2}} v(\boldsymbol{q}) \\ &\quad \times v(\boldsymbol{k}_4 - \boldsymbol{k}_5 + \boldsymbol{q}) n_{\boldsymbol{k}_5-\boldsymbol{q}} n_{\boldsymbol{k}_4+\boldsymbol{q}} n_{\boldsymbol{k}_4} \\ &= A_2 \int d^3q d^3k_4 d^3k_5 \Theta(k_\mathrm{F} - |\boldsymbol{k}_4|) \\ &\quad \times \frac{\Theta(k_\mathrm{F} - |\boldsymbol{k}_5 - \boldsymbol{q}|)\Theta(k_\mathrm{F} - |\boldsymbol{k}_4 + \boldsymbol{q}|)}{q^2 |\boldsymbol{k}_4 - \boldsymbol{k}_5 + \boldsymbol{q}|^2}.\end{aligned} \tag{B10}$$

Using a scaling analysis, we find that this integral also scales like r_s^{-2}. Employing the VEGAS [39,40] package yields

$$\mathcal{C}^{(2+,17)}(r_s) = \frac{1.73}{r_s^2}[\mathrm{Ry}]^2. \tag{B11}$$

While the contractions $\mathcal{C}^{(2+,2)}$, $\mathcal{C}^{(2+,16)}$, and $\mathcal{C}^{(2+,17)}$ above are straightforward to evaluate with *VEGAS* [39,40], the contributions $\mathcal{C}^{(2+,1)}$, $\mathcal{C}^{(2+,6)}$, $\mathcal{C}^{(2+,8)}$, $\mathcal{C}^{(2+,12)}$, $\mathcal{C}^{(2+,14)}$, and $\mathcal{C}^{(2+,15)}$ require more care, because their integrands contain factors $(v(\boldsymbol{q}))^2$, which lead to a strong divergence of the integrands in the limit $q \to 0$. In contrast, the integrals of the contractions $\mathcal{C}^{(2+,2)}$, $\mathcal{C}^{(2+,16)}$, and $\mathcal{C}^{(2+,17)}$ contain only a single factor $v(\boldsymbol{q})$, which does not produce a divergence, because it is compensated by the q^2 of $d^3q = q^2 \sin(\theta) d\theta d\phi$. However, these contributions may be grouped into pairs of two, where the two partners in a pair differ in sign. When we replace the Coulomb potential by

$$v_\eta(\boldsymbol{q}) = \frac{8\pi}{V}[\mathrm{Ry}][a_\mathrm{B}]\frac{1}{q^2 + \eta^2}, \tag{B12}$$

we observe that the limit $\eta \to 0$ is finite for the pair, while both partners in a pair diverge in this limit.

Consider for example the pair composed of $\mathcal{C}^{(2+,1)}$ and $\mathcal{C}^{(2+,14)}$. Evaluating the integrals

$$\begin{aligned}\mathcal{C}_\eta^{(2+,1)} &= 2\int \frac{d^3q d^3k_4 d^3k_5}{(2\pi)^9 n V^{-2}} v_\eta(\boldsymbol{q}) v_\eta(\boldsymbol{q}) n_{\boldsymbol{k}_5-\boldsymbol{q}} n_{\boldsymbol{k}_4+\boldsymbol{q}} \\ &= 2A_2 \int d^3q d^3k_4 d^3k_5 \Theta(k_\mathrm{F} - |\boldsymbol{k}_4 + \boldsymbol{q}|) \\ &\quad \times \frac{\Theta(k_\mathrm{F} - |\boldsymbol{k}_5 - \boldsymbol{q}|)}{[q^2 + \eta^2]^2}\end{aligned} \tag{B13}$$

and

$$\begin{aligned}\mathcal{C}_\eta^{(2+,14)} &= -2\int \frac{d^3q d^3k_4 d^3k_5}{(2\pi)^9 n V^{-2}} v_\eta(\boldsymbol{q}) v_\eta(\boldsymbol{q}) n_{\boldsymbol{k}_5-\boldsymbol{q}} n_{\boldsymbol{k}_4+\boldsymbol{q}} n_{\boldsymbol{k}_5} \\ &= 2A_2 \int d^3q d^3k_4 d^3k_5 \Theta(k_\mathrm{F} - |\boldsymbol{k}_5|) \\ &\quad \times \frac{\Theta(k_\mathrm{F} - |\boldsymbol{k}_5 - \boldsymbol{q}|)\Theta(k_\mathrm{F} - |\boldsymbol{k}_4 + \boldsymbol{q}|)}{[q^2 + \eta^2]^2}\end{aligned} \tag{B14}$$

with the VEGAS [39,40] package we obtain

$$\lim_{\eta\to 0}\left[\mathcal{C}_\eta^{(2+,1)}(r_s) + \mathcal{C}_\eta^{(2+,14)}(r_s)\right] = 2\frac{10.51}{r_s^2}[\mathrm{Ry}]^2. \tag{B15}$$

We explicitly left the spin degeneracy factor 2 in this equation.

APPENDIX C: EVALUATION OF $M_{\sigma nm}^{(3+,j)}$

In order to keep the notation simple, we discuss the contractions $\mathcal{C}_\sigma^{(3+,j)}$ for the uniform electron gas without spin polarization.

Transforming Eq. (51) into the momentum representation, we obtain the following expression for $\mathcal{C}_\sigma^{(3+,4)}$ in terms of an integral:

$$\begin{aligned}\mathcal{C}_\sigma^{(3+,4)} &= \int \frac{d^3q d^3q' d^3k_4 d^3k_5}{(2\pi)^{12} n V^{-3}} v(\boldsymbol{q}) v(\boldsymbol{q}') v(\boldsymbol{k}_4 - \boldsymbol{k}_5 + \boldsymbol{q} - \boldsymbol{q}') \\ &\quad \times n_{\boldsymbol{k}_5-\boldsymbol{q}} n_{\boldsymbol{k}_4+\boldsymbol{q}} \\ &= A_3 \int d^3q d^3q' d^3k_4 d^3k_5 \frac{1}{q^2}\frac{1}{[q']^2} \\ &\quad \times \frac{\Theta(k_\mathrm{F} - |\boldsymbol{k}_5 - \boldsymbol{q}|)\Theta(k_\mathrm{F} - |\boldsymbol{k}_4 + \boldsymbol{q}|)}{|\boldsymbol{k}_4 - \boldsymbol{k}_5 + \boldsymbol{q} - \boldsymbol{q}'|^2},\end{aligned} \tag{C1}$$

where

$$A_3 = \frac{(8\pi)^3}{(2\pi)^{12}}[\mathrm{Ry}]^3[a_\mathrm{B}]^3\frac{1}{n}. \tag{C2}$$

Scaling all momenta in Eq. (C1) by the factor ξ one may easily find that $\mathcal{C}_\sigma^{(3+,4)} \propto k_\mathrm{F}^3 \propto r_s^{-3}$. Using VEGAS [39,40], we obtain

$$\mathcal{C}_\sigma^{(3+,4)}(r_s) = -\frac{9.81}{r_s^3}[\mathrm{Ry}]^3. \tag{C3}$$

APPENDIX D: ALGORITHM TO CONSTRUCT THE SPECTRAL FUNCTION FROM NONCOMMUTING SPECTRAL MOMENT MATRICES

In this section, we provide the derivation of the algorithm described in Sec. III for the construction of the spectral function from the first four $N \times N$ spectral moment matrices, $\boldsymbol{M}^{(0)}$, $\boldsymbol{M}^{(1)}$, $\boldsymbol{M}^{(2)}$, and $\boldsymbol{M}^{(3)}$, where $\boldsymbol{M}^{(0)}$ is the unit matrix.

Assume that we manage to find Hermitian $2N\times 2N$ matrices

$$\mathcal{B}^{(1)} = \begin{pmatrix} \boldsymbol{M}^{(1)} & \boldsymbol{B}_1 \\ \boldsymbol{B}_1^\dagger & \boldsymbol{D}_1 \end{pmatrix}, \tag{D1}$$

$$\mathcal{B}^{(2)} = \begin{pmatrix} \boldsymbol{M}^{(2)} & \boldsymbol{B}_2 \\ \boldsymbol{B}_2^\dagger & \boldsymbol{D}_2 \end{pmatrix}, \tag{D2}$$

and

$$\mathcal{B}^{(3)} = \begin{pmatrix} \boldsymbol{M}^{(3)} & \boldsymbol{B}_3 \\ \boldsymbol{B}_3^\dagger & \boldsymbol{D}_3 \end{pmatrix}, \tag{D3}$$

which mutually commute, i.e.,

$$\begin{aligned} [\mathcal{B}^{(1)}, \mathcal{B}^{(2)}]_- &= 0, \\ [\mathcal{B}^{(1)}, \mathcal{B}^{(3)}]_- &= 0, \\ [\mathcal{B}^{(2)}, \mathcal{B}^{(3)}]_- &= 0, \end{aligned} \tag{D4}$$

and which satisfy

$$\mathcal{B}^{(2)} = \mathcal{B}^{(1)}\mathcal{B}^{(1)}, \tag{D5}$$

and

$$\mathcal{B}^{(3)} = \mathcal{B}^{(1)}\mathcal{B}^{(2)} = \mathcal{B}^{(1)}\mathcal{B}^{(1)}\mathcal{B}^{(1)}. \tag{D6}$$

Note that Eq. (D4) is satisfied if Eqs. (D5) and (D6) are satisfied. We will therefore solve only Eq. (D5) and Eq. (D6) below. The matrices $\boldsymbol{M}^{(I)}$, $\boldsymbol{B}_i$ and $\boldsymbol{D}_i$ have the size $N\times N$. The matrices $\boldsymbol{M}^{(I)}$ are the given Hermitian spectral moment matrices, while $\boldsymbol{B}_i$ and $\boldsymbol{D}_i$ are matrices that need to be determined such that Eqs. (D5) and (D6) are satisfied. While $\boldsymbol{D}_i$ is required to be Hermitian, $\boldsymbol{B}_i$ is not.

If we manage to find these matrices $\mathcal{B}^{(1)}$, $\mathcal{B}^{(2)}$, and $\mathcal{B}^{(3)}$, we know that they possess a common system of eigenvectors, i.e., they may be diagonalized by the same unitary transformation, because they are Hermitian and they commute mutually. Consequently, we may find a unitary transformation $\mathcal{U}$ so that

$$\mathcal{B}^{(1)} = \mathcal{U}\mathcal{D}\mathcal{U}^\dagger, \tag{D7}$$

where $\mathcal{D}$ is a diagonal matrix. Using $\mathcal{U}$ and $\mathcal{D}$ we may write

$$\mathcal{B}^{(2)} = \mathcal{U}\mathcal{D}^2\mathcal{U}^\dagger \tag{D8}$$

and

$$\mathcal{B}^{(3)} = \mathcal{U}\mathcal{D}^3\mathcal{U}^\dagger. \tag{D9}$$

In Ref. [17] we have shown that the eigenvalue problems Eqs. (D7), (D8), and (D9) may be rewritten in the form

$$\bar{\mathcal{W}}\mathcal{A}^{(I)} = \bar{\mathcal{B}}^{(I)}, \tag{D10}$$

where $I = 1, 2, 3$ (see Eq. (13) in Ref. [17]). When we denote the representation of the unit matrix as a column vector by $\bar{\mathcal{B}}^{(0)}$, we may combine Eqs. (D7), (D8), and (D9) into the compact expression

$$\bar{\mathcal{W}}\mathcal{A} = \bar{\mathcal{B}}, \tag{D11}$$

where

$$\mathcal{A} = [\mathcal{A}^{(0)}, \mathcal{A}^{(1)}, \mathcal{A}^{(2)}, \mathcal{A}^{(3)}] \tag{D12}$$

and

$$\bar{\mathcal{B}} = [\bar{\mathcal{B}}^{(0)}, \bar{\mathcal{B}}^{(1)}, \bar{\mathcal{B}}^{(2)}, \bar{\mathcal{B}}^{(3)}]. \tag{D13}$$

Next, we rewrite $\bar{\mathcal{B}}$ as

$$\bar{\mathcal{B}} = \begin{pmatrix} \mathcal{M} \\ \bar{\mathcal{B}}_{\text{Low}} \end{pmatrix} \tag{D14}$$

and

$$\bar{\mathcal{W}} = \begin{pmatrix} \mathcal{W} \\ \bar{\mathcal{W}}_{\text{Low}} \end{pmatrix}, \tag{D15}$$

where $\mathcal{M}$ and $\mathcal{W}$ are the matrices defined in Ref. [17] (see Eqs. (7) and (8) in Ref. [17]). $\mathcal{M}$ is a $N^2\times 4$ matrix, $\bar{\mathcal{B}}_{\text{Low}}$ is a $3N^2\times 4$ matrix, $\mathcal{W}$ is a $N^2\times 2N$ matrix, and $\bar{\mathcal{W}}_{\text{Low}}$ is a $3N^2\times 2N$ matrix. Thus we may rewrite Eq. (D11) as two equations:

$$\mathcal{W}\mathcal{A} = \mathcal{M} \tag{D16}$$

and

$$\bar{\mathcal{W}}_{\text{Low}}\mathcal{A} = \bar{\mathcal{B}}_{\text{Low}}. \tag{D17}$$

Equation (D16) is identical to the Eq. (9) in Ref. [17], which needs to be solved to obtain the spectral function. Thus we may solve Eq. (D16) by determining the matrices $\boldsymbol{B}_1$ and $\boldsymbol{D}_1$, and by diagonalizing the matrix $\mathcal{B}^{(1)}$.

Therefore, in order to prove the algorithm in Sec. III, it remains to show that the matrices $\boldsymbol{B}_1$ and $\boldsymbol{D}_1$ may be found by solving Eqs. (D5) and (D6). From Eq. (D5), we obtain the following equation for $\boldsymbol{B}_1$:

$$\boldsymbol{B}_1\boldsymbol{B}_1^\dagger = \boldsymbol{M}^{(2)} - \boldsymbol{M}^{(1)}\boldsymbol{M}^{(1)}. \tag{D18}$$

Since $\boldsymbol{B}_1\boldsymbol{B}_1^\dagger$ is a Hermitian matrix, it may be diagonalized:

$$\boldsymbol{B}_1\boldsymbol{B}_1^\dagger = \boldsymbol{U}\boldsymbol{D}\boldsymbol{U}^\dagger, \tag{D19}$$

where $\boldsymbol{U}$ is a unitary matrix and $\boldsymbol{D}$ is a diagonal matrix. If $\boldsymbol{B}_1\boldsymbol{B}_1^\dagger$ is positive definite, we obtain

$$\boldsymbol{B}_1 = \boldsymbol{U}\sqrt{\boldsymbol{D}}, \tag{D20}$$

which is Eq. (58) in the main text. If $\boldsymbol{B}_1\boldsymbol{B}_1^\dagger$ is not positive definite, the algorithm described in this section cannot be used. However, in all applications discussed in this paper, $\boldsymbol{B}_1\boldsymbol{B}_1^\dagger$ is positive definite. We suspect that the reason for this is that $\boldsymbol{M}^{(2+)}$ is generally positive definite.

From Eq. (D6), we obtain the following equation for $\boldsymbol{B}_2$:

$$\boldsymbol{B}_2 = [\boldsymbol{M}^{(3)} - \boldsymbol{M}^{(2)}\boldsymbol{M}^{(1)}][\boldsymbol{B}_1^\dagger]^{-1}. \tag{D21}$$

This is Eq. (59) in the main text.

From Eq. (D5), we obtain the following equation for $\boldsymbol{D}_1$:

$$\boldsymbol{D}_1 = \boldsymbol{B}_1^{-1}[\boldsymbol{B}_2 - \boldsymbol{M}^{(1)}\boldsymbol{B}_1]. \tag{D22}$$

This is Eq. (60) in the main text. $\boldsymbol{D}_1$ is required to be Hermitian, which is not directly obvious from Eq. (D22). However, making use of Eqs. (D21) and (D18) it is straightforward to show that

$$\boldsymbol{D}_1 - \boldsymbol{D}_1^\dagger = 0. \tag{D23}$$

At this point we have completely determined the matrix $\mathcal{B}^{(1)}$, from which the spectral function may be constructed using its eigenvalues, which are contained in the diagonal matrix $\mathcal{D}$, and the unitary transformation $\mathcal{U}$ defined in Eq. (D7). However, it remains to show that all those additional equations that follow from Eqs. (D5) and (D6) but that we did not

use to derive the expressions for $\boldsymbol{B}_1$ and $\boldsymbol{D}_1$ can be satisfied as well. From Eq. (D5), we obtain

$$\boldsymbol{D}_2 = \boldsymbol{B}_1^\dagger \boldsymbol{B}_1 + \boldsymbol{D}_1 \boldsymbol{D}_1, \tag{D24}$$

and from Eq. (D6), we obtain

$$\boldsymbol{B}_3 = \boldsymbol{M}^{(1)} \boldsymbol{B}_2 + \boldsymbol{B}_1 \boldsymbol{D}_2 \tag{D25}$$

and

$$\boldsymbol{D}_3 = \boldsymbol{B}_1^\dagger \boldsymbol{B}_2 + \boldsymbol{D}_1 \boldsymbol{D}_2. \tag{D26}$$

$\boldsymbol{D}_2$ as given by Eq. (D24) is Hermitian, because $\boldsymbol{D}_1$ is Hermitian according to Eq. (D23). Thus it does not violate any of the equations above. $\boldsymbol{B}_3$ as given by Eq. (D25) does not violate any of the equations above either. $\boldsymbol{D}_3$ as given by Eq. (D26) should be Hermitian, which is not directly obvious. However, using Eqs. (D24), (D22), and (D23), it is straightforward to show that

$$\boldsymbol{D}_3 - \boldsymbol{D}_3^\dagger = 0. \tag{D27}$$

Equation (65) in the main text follows from Eq. (D7), Eq. (D16), and Ref. [17].

APPENDIX E: GENERALIZATION TO MORE MOMENTS

We may generalize the argument given in Ref. [17] and show that from the first $2P$ moments ($P = 1, 2, \ldots$) one may construct the spectral function: We may map each moment $\tilde{\boldsymbol{M}}^{(I)}$ (where $\tilde{\boldsymbol{M}}^{(I)}$ denotes the moment computed from the nested commutator expression—as opposed to the moment obtained from the explicit energy integration) onto an N^2-dimensional real-valued vector $\boldsymbol{\mathcal{M}}^{(I)}$, because N^2 real-valued parameters fully define a Hermitian $N \times N$ matrix. We introduce the $N^2 \times 2P$ matrix $\boldsymbol{\mathcal{M}}$ by

$$\boldsymbol{\mathcal{M}} = [\boldsymbol{\mathcal{M}}^{(0)}, \ldots, \boldsymbol{\mathcal{M}}^{(2P-1)}]. \tag{E1}$$

We try to approximate the spectral function by

$$\frac{S_{\alpha\beta}(E)}{\hbar} = \sum_{p=1}^{P} \sum_{\gamma=1}^{N} a_{\gamma p} \mathcal{V}_{\alpha\gamma p} \mathcal{V}^*_{\beta\gamma p} \delta(E - E_{\gamma p}), \tag{E2}$$

because we expect that PN bands can be computed from the first $2P$ spectral moment matrices. Inserting this approximation into Eq. (1) yields

$$M^{(I)}_{\alpha\beta} = \sum_{p=1}^{P} \sum_{\gamma=1}^{N} a_{\gamma p} \mathcal{W}_{\alpha\beta\gamma p} [E_{\gamma p}]^I, \tag{E3}$$

where we defined $\mathcal{W}_{\alpha\beta\gamma p} = \mathcal{V}_{\alpha\gamma p} \mathcal{V}^*_{\beta\gamma p}$. We may consider $\mathcal{W}_{\alpha\beta\gamma p}$ as the row-α column-β element of a Hermitian matrix $\boldsymbol{\mathcal{W}}_{\gamma p}$. Since $\gamma = 1, \ldots, N$ and $p = 1, \ldots, P$, there are PN such matrices. As the Hermitian $N \times N$ matrix $\boldsymbol{\mathcal{W}}_{\gamma p}$ is equivalent to a N^2-dimensional real-valued vector $\tilde{\boldsymbol{\mathcal{W}}}_{\gamma p}$, we define the $N^2 \times PN$ matrix $\boldsymbol{\mathcal{W}} = [\tilde{\boldsymbol{\mathcal{W}}}_{11} \ldots \tilde{\boldsymbol{\mathcal{W}}}_{NP}]$. Additionally, we construct the $PN \times 2P$ matrix $\boldsymbol{\mathcal{A}}$ by setting the element $\mathcal{A}_{\gamma p m}$ in row (γ, p) and column m to $a_{\gamma p} (E_{\gamma p})^{m-1}$. The requirements $\boldsymbol{M}^{(I)} = \tilde{\boldsymbol{M}}^{(I)}$ with $I = 0, 1, \ldots 2P - 1$ (where $\tilde{\boldsymbol{M}}^{(I)}$ are the moments computed from the nested commutator expressions) can now be formulated in compact form by

$$\boldsymbol{\mathcal{W}} \boldsymbol{\mathcal{A}} = \boldsymbol{\mathcal{M}}. \tag{E4}$$

This is the generalization of Eq. (9) in Ref. [17] for the first $2P$ moments. The form of the equation is the same, only the sizes of the matrices are different. Since the matrix $\boldsymbol{\mathcal{M}}$ contains $2PN^2$ elements, Eq. (E4) defines $2PN^2$ nonlinear equations. Each vector $\boldsymbol{\mathcal{V}}_{\gamma p}$ has N components and there are PN such vectors. $\boldsymbol{\mathcal{V}}_{\gamma p}$ is required to be normalized and the gauge-transformation $\boldsymbol{\mathcal{V}}_{\gamma p} \to e^{i\Phi} \boldsymbol{\mathcal{V}}_{\gamma p}$ does not affect $\mathcal{W}_{\alpha\beta\gamma p} = \mathcal{V}_{\alpha\gamma p} \mathcal{V}^*_{\beta\gamma p}$. Thus every $\boldsymbol{\mathcal{V}}_{\gamma p}$ is determined by $2(N-1)$ real-valued unknowns, i.e., $2P(N^2 - N)$ unknown coefficients need to be found to determine all vectors $\boldsymbol{\mathcal{V}}_{\gamma p}$. Additionally, we need to find the PN energies $E_{\gamma p}$ as well as the PN spectral weights $a_{\gamma p}$. Consequently, Eq. (E4) is a system of $2PN^2$ nonlinear equations for $2PN^2$ unknowns. Thus one may expect that it should be possible to compute PN bands from the first $2P$ spectral moment matrices of size $N \times N$, because the number of unknowns matches the number of available nonlinear equations.

[1] P. Hohenberg and W. Kohn, Inhomogeneous electron gas, Phys. Rev. **136**, B864 (1964).

[2] W. Kohn and L. J. Sham, Self-consistent equations including exchange and correlation effects, Phys. Rev. **140**, A1133 (1965).

[3] J. Sánchez-Barriga, J. Fink, V. Boni, I. Di Marco, J. Braun, J. Minár, A. Varykhalov, O. Rader, V. Bellini, F. Manghi, H. Ebert, M. I. Katsnelson, A. I. Lichtenstein, O. Eriksson, W. Eberhardt, and H. A. Dürr, Strength of Correlation Effects in the Electronic Structure of Iron, Phys. Rev. Lett. **103**, 267203 (2009).

[4] Y. Yao, L. Kleinman, A. H. MacDonald, J. Sinova, T. Jungwirth, D.-S. Wang, E. Wang, and Q. Niu, First Principles Calculation of Anomalous Hall Conductivity in Ferromagnetic bcc Fe, Phys. Rev. Lett. **92**, 037204 (2004).

[5] K. Gilmore, Y. U. Idzerda, and M. D. Stiles, Identification of the Dominant Precession-Damping Mechanism in Fe, Co, and Ni by First-Principles Calculations, Phys. Rev. Lett. **99**, 027204 (2007).

[6] F. Freimuth, S. Blügel, and Y. Mokrousov, Direct and inverse spin-orbit torques, Phys. Rev. B **92**, 064415 (2015).

[7] M. Berritta, R. Mondal, K. Carva, and P. M. Oppeneer, *Ab Initio* Theory of Coherent Laser-Induced Magnetization in Metals, Phys. Rev. Lett. **117**, 137203 (2016).

[8] J. Ibañez-Azpiroz, S. S. Tsirkin, and I. Souza, Ab initio calculation of the shift photocurrent by Wannier interpolation, Phys. Rev. B **97**, 245143 (2018).

[9] L. Hedin, New method for calculating the one-particle green's function with application to the electron-gas problem, Phys. Rev. **139**, A796 (1965).

[10] C. Franz, F. Freimuth, A. Bauer, R. Ritz, C. Schnarr, C. Duvinage, T. Adams, S. Blügel, A. Rosch, Y. Mokrousov, and C. Pfleiderer, Real-Space and Reciprocal-Space Berry Phases in the Hall Effect of $Mn_{1-x}Fe_xSi$, Phys. Rev. Lett. **112**, 186601 (2014).

[11] I. A. Nekrasov, G. Keller, D. E. Kondakov, A. V. Kozhevnikov, T. Pruschke, K. Held, D. Vollhardt, and V. I. Anisimov, Comparative study of correlation effects in $CaVO_3$ and $SrVO_3$, Phys. Rev. B **72**, 155106 (2005).

[12] A. Liebsch, Effect of Self-Energy Corrections on the Valence-Band Photoemission Spectra of Ni, Phys. Rev. Lett. **43**, 1431 (1979).

[13] W. Nolting, W. Borgiel, V. Dose, and T. Fauster, Finite-temperature ferromagnetism of nickel, Phys. Rev. B **40**, 5015 (1989).

[14] J. Kolorenč, A. I. Poteryaev, and A. I. Lichtenstein, Valence-band satellite in ferromagnetic nickel: LDA+DMFT study with exact diagonalization, Phys. Rev. B **85**, 235136 (2012).

[15] A. Georges, G. Kotliar, W. Krauth, and M. J. Rozenberg, Dynamical mean-field theory of strongly correlated fermion systems and the limit of infinite dimensions, Rev. Mod. Phys. **68**, 13 (1996).

[16] G. Kotliar, S. Y. Savrasov, K. Haule, V. S. Oudovenko, O. Parcollet, and C. A. Marianetti, Electronic structure calculations with dynamical mean-field theory, Rev. Mod. Phys. **78**, 865 (2006).

[17] F. Freimuth, S. Blügel, and Y. Mokrousov, Construction of the spectral function from noncommuting spectral moment matrices, Phys. Rev. B **106**, 045135 (2022).

[18] G. Geipel and W. Nolting, Ferromagnetism in the strongly correlated Hubbard model, Phys. Rev. B **38**, 2608 (1988).

[19] H. Eskes, A. M. Oleś, M. B. J. Meinders, and W. Stephan, Spectral properties of the Hubbard bands, Phys. Rev. B **50**, 17980 (1994).

[20] W. Nolting, A. Vega, and T. Fauster, Electronic quasiparticle structure of ferromagnetic bcc iron, Z. Phys. B **96**, 357 (1995).

[21] O. K. Kalashnikov and E. S. Fradkin, The spectral density method applied to systems showing phase transitions, Phys. Status Solidi B **59**, 9 (1973).

[22] S. R. White, Spectral weight function for the two-dimensional Hubbard model, Phys. Rev. B **44**, 4670 (1991).

[23] V. Turkowski and J. K. Freericks, Nonequilibrium sum rules for the retarded self-energy of strongly correlated electrons, Phys. Rev. B **77**, 205102 (2008).

[24] W. Nolting and W. Brewer, *Fundamentals of Many-body Physics: Principles and Methods* (Springer, Berlin, Heidelberg, 2009).

[25] J. P. Perdew and Y. Wang, Accurate and simple analytic representation of the electron-gas correlation energy, Phys. Rev. B **45**, 13244 (1992).

[26] J. P. Perdew and A. Zunger, Self-interaction correction to density-functional approximations for many-electron systems, Phys. Rev. B **23**, 5048 (1981).

[27] J. Heyd, G. E. Scuseria, and M. Ernzerhof, Hybrid functionals based on a screened Coulomb potential, J. Chem. Phys. **118**, 8207 (2003).

[28] D. M. Ceperley and B. J. Alder, Ground State of the Electron Gas by a Stochastic Method, Phys. Rev. Lett. **45**, 566 (1980).

[29] M. Gell-Mann and K. A. Brueckner, Correlation energy of an electron gas at high density, Phys. Rev. **106**, 364 (1957).

[30] W. Eberhardt and E. W. Plummer, Angle-resolved photoemission determination of the band structure and multielectron excitations in Ni, Phys. Rev. B **21**, 3245 (1980).

[31] D. E. Eastman, F. J. Himpsel, and J. A. Knapp, Experimental Band Structure and Temperature-Dependent Magnetic Exchange Splitting of Nickel Using Angle-Resolved Photoemission, Phys. Rev. Lett. **40**, 1514 (1978).

[32] A. K. See and L. E. Klebanoff, Spin-resolved x-ray photoemission from ferromagnetic nickel, Phys. Rev. B **51**, 11002 (1995).

[33] A. I. Lichtenstein, M. I. Katsnelson, and G. Kotliar, Finite-Temperature Magnetism of Transition Metals: An *ab initio* Dynamical Mean-Field Theory, Phys. Rev. Lett. **87**, 067205 (2001).

[34] I. Inoue, I. Hase, Y. Aiura, A. Fujimori, K. Morikawa, T. Mizokawa, Y. Haruyama, T. Maruyama, and Y. Nishihara, Systematic change of spectral function observed by controlling electron correlation in $Ca_{1-x}Sr_xVO_3$ with fixed $3d^1$ configuration., Physica C **235-240**, 1007 (1994).

[35] A. Sekiyama, H. Fujiwara, S. Imada, S. Suga, H. Eisaki, S. I. Uchida, K. Takegahara, H. Harima, Y. Saitoh, I. A. Nekrasov, G. Keller, D. E. Kondakov, A. V. Kozhevnikov, T. Pruschke, K. Held, D. Vollhardt, and V. I. Anisimov, Mutual Experimental and Theoretical Validation of Bulk Photoemission Spectra of $Sr_{1-x}Ca_xVO_3$, Phys. Rev. Lett. **93**, 156402 (2004).

[36] B. Amadon, F. Lechermann, A. Georges, F. Jollet, T. O. Wehling, and A. I. Lichtenstein, Plane-wave based electronic structure calculations for correlated materials using dynamical mean-field theory and projected local orbitals, Phys. Rev. B **77**, 205112 (2008).

[37] M. Potthoff, T. Herrmann, T. Wegner, and W. Nolting, The moment sum rule and its consequences for ferromagnetism in the Hubbard model, Phys. Status Solidi B **210**, 199 (1998).

[38] W. Nolting and A. M. Oles, Spectral density approach for the quasiparticle concept in the s-f model (ferromagnetic semiconductors), J. Phys. C **13**, 2295 (1980).

[39] G. Peter Lepage, A new algorithm for adaptive multidimensional integration, J. Comput. Phys. **27**, 192 (1978).

[40] G. P. Lepage, Adaptive multidimensional integration: VEGAS enhanced, J. Comput. Phys. **439**, 110386 (2021).